ORIGINAL RESEARCH

Gold nanoparticles affect the antioxidant status in selected normal human cells

Noami Daems[1]
Sébastien Penninckx[2]
Inge Nelissen[3]
Karen Van Hoecke[4]
Thomas Cardinaels[4,5]
Sarah Baatout[1]
Carine Michiels[6]
Stéphane Lucas[2]
An Aerts[1]

[1]Radiobiology Research Unit, Interdisciplinary Biosciences, Institute for Environment, Health and Safety, Belgian Nuclear Research Centre (SCK.CEN), Mol, Belgium; [2]Research Center for the Physics of Matter and Radiation-NARILIS, University of Namur, Namur, Belgium; [3]Health Department, Flemish Institute For Technological Research (VITO), Mol, Belgium; [4]Radiochemistry Expert Group, Institute for Nuclear Materials Science, Belgian Nuclear Research Centre (SCK. CEN), Mol, Belgium; [5]Department of Chemistry, KU Leuven, Heverlee, Belgium; [6]Unité de Recherche en Biologie Cellulaire-NARILIS, University of Namur, Namur, Belgium

Correspondence: An Aerts
Belgian Nuclear Research Centre (SCK. CEN), Boeretang 200, 2400 Mol, Belgium
Tel +32 1 433 2930
Email an.aerts@sckcen.be

Purpose: This study evaluates the cytotoxicity of AuNPs coated with polyallylamine (AuNPs-PAA) and conjugated or not to the epidermal growth factor receptor (EGFR)-targeting antibody Cetuximab (AuNPs-PAA-Ctxb) in normal human kidney (HK-2), liver (THLE-2) and microvascular endothelial (TIME) cells, and compares it with two cancer cell lines that are EGFR-overexpressing (A431) or EGFR-negative (MDA-MB-453).

Results: Conjugation of Cetuximab to AuNPs-PAA increased the AuNPs-PAA-Ctxb interactions with cells, but reduced their cytotoxicity. TIME cells exhibited the strongest reduction in viability after exposure to AuNPs-PAA(±Ctxb), followed by THLE-2, MDA-MB-453, HK-2 and A431 cells. This cell type-dependent sensitivity was strongly correlated to the inhibition of thioredoxin reductase (TrxR) and glutathione reductase (GR), and to the depolarization of the mitochondrial membrane potential. Both are suggested to initiate apoptosis, which was indeed detected in a concentration- and time-dependent manner. The role of oxidative stress in AuNPs-PAA(±Ctxb)-induced cytotoxicity was demonstrated by co-incubation of the cells with N-acetyl L-cysteine (NAC), which significantly decreased apoptosis and mitochondrial membrane depolarization.

Conclusion: This study helps to identify the cells and tissues that could be sensitive to AuNPs and deepens the understanding of the risks associated with the use of AuNPs in vivo.

Keywords: cytotoxicity, EGFR, Cetuximab, oxidative stress

Introduction

In order to improve cancer detection and therapy efficiency, gold nanoparticles (AuNPs) are emerging as promising contrast agents, drug delivery vehicles, photo-thermal agents and radiosensitizers.[1–9] Functional surface modifications are typically applied to actively target the cancer cells.[10–13] In our team, 5 nm AuNPs are synthesized and coated with organic polyallylamine (AuNPs-PAA) by plasma vapor deposition. AuNPs-PAA are subsequently conjugated to Cetuximab (AuNPs-PAA-Ctxb), a commercially available antibody targeting the epidermal growth factor receptor (EGFR), which is overexpressed in numerous tumor types.[14] The resulting nanoconjugates are able to selectively target EGFR-overexpressing cancer cells in vitro and in vivo, and exhibit an in vivo pharmacokinetic profile similar to that of unconjugated Cetuximab. However, the reticuloendothelial system (RES) in the liver and spleen rapidly sequestrates AuNPs-PAA-Ctxb.[15,16] This phenomenon has been demonstrated by several other in vivo biodistribution studies and is the main reason why clinical success of AuNPs remains, in general, elusive.[15,17–22] In addition, accumulation of AuNPs-PAA-Ctxb and other AuNPs has been demonstrated in the kidneys, which are particularly sensitive to xenobiotics due to their

high degree of vascularization and their ability to concentrate toxins.[15–17,23–26] In conclusion, since AuNPs accumulate in several non-target organs in vivo, it is essential to assess the potential toxicity of AuNPs in these healthy cells and tissues before AuNPs can be used in a clinical setting.[27]

Due to their small size, nanoparticles generally exhibit different characteristics and have a higher reactivity compared to their bulk counterparts. Various studies have reported that AuNPs are able to induce formation of reactive oxygen species (ROS) in cells, which would be the major cause of cellular damage, genotoxicity and cell death.[28–30] In addition, abnormalities in tissue morphology of the kidney, the liver and the spleen and a minor increase in lung inflammation were detected in rodents after exposure to AuNPs.[24,31–34] However, these findings contradict to those of other research groups that have demonstrated that AuNPs exhibit no toxic health effects at all in vitro and in vivo.[35–37] These conflicting results in the literature indicate that it is difficult to predict the toxicity of AuNPs in different biological systems, and that this depends strongly on their physicochemical properties including particle size, shape, surface coating, surface charge and adsorbed protein corona.[36,38–42]

In this study, we characterized our in-house produced AuNPs-PAA and AuNPs-PAA-Ctxb in terms of their size and surface charge. Furthermore, we evaluated and compared the cellular uptake and cytotoxic effects of the AuNPs-PAA and AuNPs-PAA-Ctxb on human microvascular endothelial (TIME) cells, human proximal tubular kidney (HK-2) cells and human liver (THLE-2) cells. These three cell types were chosen because they originate from normal human primary cells, retaining their phenotypic and functional characteristics. Furthermore, since these cell types are exposed to a significant amount of AuNPs in vivo, they are suitable in vitro models for the estimation and understanding of the nanoparticle toxicity on human health, such as vascular toxicity, nephrotoxicity and hepatotoxicity.[15,17–22] Indeed, microvascular endothelial cells are the first cells to encounter the AuNPs after intravenous injections and are responsible for the transport and exchange of the AuNPs from the bloodstream to the tissues. Renal tubular cells are exposed to AuNPs after their filtration through the glomerular capillary wall during renal excretion. Finally, although Kupffer cells in the liver have a high phagocytic capacity to sequestrate AuNPs, the hepatocytes are part of the hepatobiliary system, which represents an important pathway for nanoparticle processing and thus forms a potential site for toxicity.[43] In addition to these non-cancerous cell types, EGFR-overexpressing A431 cells and EGFR-negative MDA-MB-453 cancer cell lines were used as positive and negative controls, respectively, for antibody targeting. Cytotoxicity was assessed by following the number of viable cells and measuring the mitochondrial membrane potential, the thioredoxin reductase and glutathione reductase activity, and the extent of apoptotic cell death. In order to explore the role of oxidative stress, the possible protective effect of N-acetyl L-cysteine (NAC) was studied. If a situation applies for both AuNPs-PAA and AuNPs-PAA-Ctxb, we will refer to them as AuNPs-PAA(±Ctxb) in the remainder of the manuscript. This work contributes to a better estimation of the potential negative effects of therapeutic AuNPs formulations on human health.

Materials and methods
Chemicals
Polyallylamine, (1-Cyano-2-ethoxy-2-oxoethylidenaminooxy) dimethylamino-morpholino-carbenium hexafluorophosphate (COMU), Arabic gum, NAC, CelLytic M, the bicinchoninic acid (BCA) protein assay kit, the Thioredoxin reductase assay kit, bovine serum albumin (BSA), non-fat dry milk, phosphatase inhibitor tablets (PhosStop) and the Complete Mini EDTA-free Protease Inhibitor Cocktail were purchased from Sigma-Aldrich (Diegem, Belgium). Cetuximab (Erbitux® 5 mg/ml) was kindly provided by the Sint-Dimpna Hospital (Geel, Belgium). Vivaspin® centrifugal concentrators and cacodylate buffer were obtained from Merck (Overijse, Belgium). All cell lines, the Microvascular Endothelial Cell Growth Kit-VEGF and EGF were obtained from ATCC (Molsheim Cedex, France). Fetal bovine serum (FBS), Dulbecco's modified Eagle's medium (DMEM), DMEM:F12, phosphate buffered saline (PBS) tablets and penicillin-streptomycin were purchased from Gibco (Aalst, Belgium). The BEGM Bullet Kit was received from Lonza (Verviers, Belgium). The CellTiter 96 Aqueous One Solution Cell Proliferation Assay was purchased from Promega (Leiden, The Netherlands). The IncuCyte Caspase 3/7 Green Reagent and the IncuCyte Annexin V Red Reagent were obtained from Essen BioScience (Hertfordshire, UK). TGX Stain-free Precast Protein Gels, Trans-Blot Turbo Mini Nitrocellulose Transfer Packs and the Clarity Western ECL substrate kit were provided by Bio-Rad Laboratories (Temse, Belgium). The rabbit anti-EGFR antibody was purchased from Cell Signaling Technology (Leiden, The Netherlands). The

mouse anti-β actin antibody was purchased from Santa Cruz Biotechnology (Heidelberg, Germany). HRP-labeled goat anti-rabbit antibody, goat-anti mouse antibody and tetramethylrhodamine, methyl ester, perchlorate (TMRM) were obtained from Invitrogen (Merelbeke, Belgium). Glutaraldehyde and osmic acid were received from Agar Scientific (Essex, UK). The Eponate 12 Embedding Kit with BDMA was purchased from Ted Pella (Paris, France). The Glutathione Reductase Assay kit was obtained from Abcam (Cambridge, UK). Nitric acid (HNO_3), hydrochloric acid (HCl), hydrogen peroxide (H_2O_2) and hydrofluoric acid (HF) were of trace metal grade and purchased from Fisher Scientific (Merelbeke, Belgium). SPEX Certiprep certified standard solutions (Boom B.V., Meppel, The Netherlands) were used to prepare the calibration standards and internal standards.

Production of AuNPs-PAA and Cetuximab conjugation

The AuNPs were produced and coated with PAA by physical plasma vapor deposition as described previously.[14] The resulting PAA-coated AuNPs (AuNPs-PAA) were dispersed in acetate buffer (pH 5) under pulsed sonication (50 W, 30 kHz, 20% amplitude, 0.5 sec pulses), and were subsequently purified from excess PAA and NaCl by filtration in a centrifugal filter unit with a molecular cut-off of 10 kDa. Cetuximab was purified by filtration in a centrifugal filter unit with a molecular cut-off of 10 kDa, after which it was lyophilized (LABCONCO, Osterode, Germany). Lyophilized Cetuximab and COMU were dissolved in 0.01 M PBS to a concentration of 1 mg/mL and 1.5 mg/mL, respectively. The Cetuximab and COMU solutions were mixed and the pH was adjusted to 7 with 0.1 M HCl. Then, the AuNPs-PAA were added to the Cetuximab-COMU mixture to achieve a final concentration of 0.24 mg/ml, 0.43 mg/mL and 0.17 mg/mL of Cetuximab, COMU and gold, respectively. The mixture was stirred for 4 h at room temperature, after which it was purified with a centrifugal filter unit with a molecular cut-off of 300 kDa. The AuNPs-PAA-Ctxb were lyophilized for long-term storage after the addition of 3% arabic gum as stabilizer, which also causes steric repulsion between the nanoparticles when they are re-suspended after the freeze-drying process.

Nanoparticle characterization (Zeta potential and size distribution)

Lyophilized AuNPs-PAA(±Ctxb) were dispersed in Class 1 water, DMEM or DMEM with 10% (v/v) FBS to a gold concentration of 80 µg/ml. The size distribution of the nanoparticles was characterized by means of CPS Disc Centrifugation (Benelux Scientific, Eke, Belgium). A rotational speed of 22,000 r.p.m., a sucrose density gradient of 2–8% with a fluid density of 1.017 g/mL and a refractive index of 1.341 were employed. The measurement range of the instrument was set from 3.5 nm to 50 µm. The particle density was set to 10.05 g/mL and the particle refractive index to 0.47. Each measurement was calibrated with certified PVC microparticles provided by CPS Instruments, having a peak diameter of 0.263 µm and a particle density of 1.386 g/ml. The peak particle sizes and the 5th and 95th percentiles were extracted from relative number size distributions. The zeta potential was determined with the Nanosizer Nano ZSP (Malvern P analytical, Brussels, Belgium) with a temperature equilibration time of 2 min at 25 °C. A dispersant refractive index of 1.330, a viscosity of 0.8872 cP and a dispersant dielectric constant of 78.5 were used. UV-Vis spectra were recorded on the CLARIOstar microplate reader (BMS Labtech, De Meern, Netherlands). Conjugation of Cetuximab to AuNPs-PAA was also confirmed by SDS-PAGE. 10 µg of Cetuximab, Cetuximab + AuNPs-PAA and AuNPs-PAA-Ctxb were loaded on a TGX Stain-free Precast Protein Gel. Migrated Cetuximab was detected with UV light by using the Fusion FX Imager (Vilber Lourmat, Eberhardzell, Germany).

Cell culture

A431 cells and MDA-MB-453 cells were grown in DMEM High Glucose medium. HK-2 cells were grown in DMEM:F12 High Glucose medium. TIME cells were grown in Vascular Cell Basal Medium supplemented with the Microvascular Endothelial Cell Growth Kit-VEGF. Finally, THLE-2 cells were cultured by using the BEGM Bullet kit without gentamycin/amphotericin and epinephrine, but supplemented with 5 ng/mL EGF. All the cultured cells were supplemented with 10% FBS and 100 u/mL penicillin-streptomycin and were maintained in a humidified 37 °C incubator with 5% CO_2.

MTS viability assay

The cell viability after exposure to AuNPs-PAA(±Ctxb) was tested with the CellTiter 96 AQueous One Solution Cell Proliferation Assay. Cells were seeded into a 96-well plate (25,000 cells/cm^2 for HK-2 and TIME cells; 28,125 cells/cm^2 for A431 cells; 31,250 cells/cm^2 for THLE-2 cells; and 43,750 cells/cm^2 for MDA-MB-453

cells). After 24 h, the medium was replaced by fresh medium containing increasing concentrations of nanoparticles (1.56–50.00 µg Au/mL) for incubation periods of 3 h or 24 h. After the exposure period, the medium was discarded and cells were washed twice with DMEM +10% FBS to avoid the interference of the AuNPs at 490 nm. The MTS reagent, prepared according to the manufacturer's instructions, was added to the cells. The plate was incubated at 37 °C for 1.5 h and the absorbance was measured at 490 nm with the CLARIOstar microplate reader (BMS Labtech, De Meern, Netherlands). The cell viability was calculated as the ratio of the absorbance of the sample well to the average of the unexposed control wells, after subtraction of the background signal of wells that contained AuNPs-PAA(±Ctxb) but no cells. The results, expressed as percentages, were obtained from at least three independent experiments with a minimum of three replicates per condition. Curve fitting of the concentration-response data was performed with Origin 2017 software, by using a log-logistic function and a modified log-logistic function (Equation S1 and Equation S2, respectively).

Live cell imaging

The effect of AuNPs-PAA(±Ctxb) on cell apoptosis was investigated by recording time-lapse images of the cells every 2 h during 3 days with the IncuCyte ZOOM system (Essen BioScience, Hertfordshire, UK). Approximately 15,000–45,000 cells/cm^2 were seeded into 96-well plates. After 24 h, the medium was replaced by fresh medium containing increasing concentrations of nanoparticles (1.56–50.00 µg Au/mL). To assess the presence of oxidative stress, cells were also co-incubated with 2 nM NAC. The IncuCyte Caspase 3/7 Green Reagent and the IncuCyte Annexin V Red Reagent were added to the cell media to monitor apoptosis according to the manufacturer's instructions. Built-in software was used to analyze the images in order to generate the annexin V and caspase 3/7 area data (µm^2/well), which was normalized to cell confluency data (%). The results were obtained from at least three replicates per condition.

Western blot analysis

To determine EGFR expression, cells were cultured in T25 flasks until 80% confluency. Briefly, cells were rinsed with ice cold PBS and lysed with lysis buffer (20 mM Tris, 150 mM NaCl, 1 mM EDTA, 1 mM EGTA, 1% sodium deoxycholate, 1% Nonidet P40, 10% glycerol, pH 7.5)

containing a protease and phosphatase inhibitor tablet. The protein concentrations were quantified with the BCA kit according to the manufacturer's instructions. 15 µg of proteins were separated on a 4TGX Stain-free Precast Protein Gel. After protein transfer onto a nitrocellulose membrane, the membranes were blocked with 5% non-fat dry milk in PBS-0.1% Tween (PBS-T) for 2 h at room temperature. Next, membranes were incubated with rabbit anti-EGFR antibody diluted 1:1,000 in 5% BSA, or with mouse anti-β-actin antibody diluted 1:5,000 in 5% non-fat dry milk, overnight at 4 °C. After washing in PBS-T, the membranes were incubated with HRP-labeled goat anti-rabbit antibody diluted 1:10,000 in 5% BSA or HRP-labeled goat anti-mouse antibody diluted 1:50,000 in 5% non-fat dry milk for 1 h at room temperature. Protein detection was performed with the Clarity Western ECL substrate kit and the Fusion FX Imager (Vilber Lourmat, Eberhardzell, Germany). Protein bands were quantified with Bio1D analysis software (Vilber Lourmat, Eberhardzell, Germany). The EGFR protein level was normalized to the level of the housekeeping protein, β-actin. The results are expressed as mean EGFR expression relative to the EGFR expression in A431 cells and were obtained from at least 4 independent replicates.

Transmission electron microscopy and energy dispersive x-ray spectroscopy

Transmission electron microscopy (TEM) was used to determine the subcellular localization of the AuNPs-PAA-Ctxb. Approximately 25,000–45,000 cells/cm^2 were seeded in T175 flasks. After 24 h, the medium was replaced by fresh medium containing 5.0 µg Au/mL of AuNPs-PAA-Ctxb for incubation periods of 3 h or 24 h. After the exposure period, the cells were washed twice with DMEM +10% FBS, once with PBS, and collected by trypsinization. Cells were fixed with 2.5% (w/v) glutaraldehyde in 0.1 M cacodylate buffer (pH 7.4) at 4 °C during 2.5 h. Next, the cells were washed with 0.2 M cacodylate buffer and subsequently post-fixed in 1% (v/w) osmic acid in 0.1 M cacodylate buffer. Finally, samples were dehydrated by successive passages in increasing concentrations of ethanol (30%, 50%, 70%, 85% and 100%), and were embedded in resin. Ultra-thin sections for TEM analysis were prepared with an 8,800 ultratome III (LKB, Sollentuna, Sweden), after which the cells were visualized with a FEI Tecnai 10 TEM (Thermo Fisher Scientific, Zaventem, Belgium) and iTEM software (Olympus, Soft

Imaging Solutions, Muenster, Germany). Energy dispersive X-ray spectroscopy (EDS) was performed on representative cells with the scanning electron microscope JEOL 7500F and Jeol JED2300 software (Jeol Benelux, Zaventem, Belgium).

Inductively coupled plasma mass spectrometry

Inductively coupled plasma mass spectrometry (ICP-MS) was used to quantify the cellular gold content after interaction of AuNPs-PAA(±Ctxb) with the cells. Approximately 20,000–40,000 cells/cm^2 were seeded in T25 flasks. After 24 h, the medium was replaced by fresh medium containing 5.0 µg Au/mL of AuNPs-PAA(±Ctxb) for incubation periods of 3 h, 6 h, 12 h or 24 h. After exposure, the cells were rinsed twice with DMEM +10% FBS, once with PBS, and collected by trypsinization. Detached cells were washed twice with DMEM +10% FBS by successive centrifugation. The cells were counted and re-suspended in 1 ml of Class 1 water. Next, samples were digested with 0.5 ml aqua regia for 2 h at 110 °C in PFA Savillex® digestion vessels (VWR, Leuven, Belgium). The samples were evaporated to incipient dryness, redissolved in 5% HNO$_3$ and then exposed to UV light in a 705 UV-digester (Metrohm, Zwijndrecht, Belgium) for 2 h. Beforehand, 100 µL of 30% H$_2$O$_2$ was added as initiator for the UV digestion. Finally, 0.05% HF was added to reduce Au memory effects. The Au content in the samples was determined with an XSeriesII quadrupole ICP-MS instrument (ThermoFisher Scientific, Bremen, Germany). Data was acquired from 20 ms dwell time per isotope, 200 sweeps per reading, and 5 readings per sample, resulting in 20 s of measurement time per isotope. A rinsing time of 150 s was included between each sample. The elements Re, Ir, Tl were used as internal standards. An external calibration curve based on 0.5–1–2–5 ng/mL of Au standards permitted quantification of the gold content in the samples. The results are expressed as mean pg Au/cell calculated from three replicates per condition obtained from one experiment.

TMRM assay

The effect of AuNPs-PAA(±Ctxb) on the mitochondrial membrane potential was assessed by measuring the mitochondrial retention of the TMRM dye. Approximately 25,000 cells/cm^2 were seeded in 24-well plates. After 24 h, the medium was replaced by fresh medium containing a non-lethal concentration of nanoparticles (ie 3.0 µg

Au/mL for TIME cells, and 5.0 µg Au/mL for THLE-2 and HK-2 cells) for incubation periods of 30 min, 3 h, 6 h, 12 h or 24 h. The non-lethal concentration was estimated on the basis of IncuCyte apoptosis data acquired from cells exposed to AuNPs-PAA. To assess the presence of oxidative stress after 12 h of exposure, cells were also co-incubated with 2 nM NAC. After the exposure period, the cells were washed twice with DMEM +10% FBS, once with PBS, and collected by trypsinization. Subsequently, cells were re-suspended in full medium containing 100 nM TMRM dye, and incubated for 20 min at 37 °C. After centrifugation, cells were re-suspended in PBS, and the TMRM intensity was measured in the FL2-channel of the BD Accuri C6 flow cytometer (BD Biosciences, Erembodegem, Belgium). The relative average TMRM intensity was calculated as the ratio of the TMRM intensity of the sample wells to the average TMRM intensity of the unexposed control wells, after subtraction of the background signal from unlabeled cells. The results were obtained from at least three independent experiments with a minimum of three replicates per condition.

Thioredoxin reductase and glutathione reductase activity measurements

Approximately 25,000–45,000 cells/cm^2 cells were seeded in 175 cm^2 flasks. After 24 h, the medium was replaced by fresh medium containing a non-lethal concentration of nanoparticles (ie 3.0 µg Au/mL for TIME cells and 5.0 µg Au/mL for THLE-2 and HK-2 cells) for an incubation period of 12 h. The non-lethal concentration was estimated on the basis of IncuCyte apoptosis data acquired from cells exposed to AuNPs-PAA. After the exposure period, cells were washed twice with DMEM +10% FBS, once with PBS, and collected by tryspinization. Subsequently, the cell pellets were re-suspended in ice cold PBS. Next, the cells were centrifuged and lysed by CelLytic M (100 µl per 10^7 cells), supplemented with a protease inhibitor tablet. After centrifugation of the samples (14 000 g, 10 min, 4 °C), protein concentrations were quantified with the BCA protein assay kit. Next, the thioredoxin reductase activity and the glutathione reductase activity in 100 µg of protein were measured according to the manufacturer's instructions. Results are expressed as the average change in absorbance per minute and are obtained from at least three independent experiments with a minimum of two replicates per condition.

Statistical analysis

Results are reported as mean ± standard error (SE). One-way ANOVA was performed to compare cell groups exposed to different concentrations of AuNPs-PAA (±Ctxb), or exposed for different periods of time, with the unexposed control group, followed by a Dunnett post-hoc test. Two-way ANOVA was used to analyze the IncuCyte data in order to compare cell groups exposed to different concentrations of AuNPs-PAA(±Ctxb) with the unexposed control group as a function of time, followed by a Dunnett post-hoc test. A Student's t-test was used to compare the means of two groups. For the ICP-MS data, a Kruskal-Wallis test and a Dunn's post-hoc test were performed to compare cell groups exposed for different periods of time. A Mann-Whitney test was used to compare the means of two groups. The statistical analyses were performed by using Prism 7.02 software. The level of statistical significance is depicted by the number of asterisks as follows: $*p<0.05$, $**p<0.01$, $***p<0.001$, $****p<0.0001$.

Results
Size distribution and zeta potential of AuNPs-PAA(±Ctxb)

First, UV-Vis spectra showed surface plasmon resonance peaks between 522 and 526 nm, which is characteristic for nano-sized AuNPs (Figure S1A). The composition of the AuNPs-PAA-Ctxb and the preserved functionality of Cetuximab after conjugation were described previously.[16,44] Successful conjugation of Cetuximab was also demonstrated by gel electrophoresis showing that Cetuximab was unable to migrate when conjugated to AuNPs-PAA, unlike uncoupled Cetuximab incubated with AuNPs-PAA (Figure S1B). Next, the AuNPs-PAA(±Ctxb) were characterized in terms of their size distribution and nanoparticle surface charge. Both these parameters were determined for the AuNPs-PAA(±Ctxb) dispersed in Class 1 water, DMEM and DMEM supplemented with 10% FBS (Table 1). Size measurements demonstrated peak particle diameters of 4–5 nm for AuNPs-PAA when dispersed in Class 1 water, DMEM and DMEM with 10% FBS. Conjugation of AuNPs-PAA to Cetuximab increased the peak particle diameter to 26 nm, 25 nm and 19 nm when dispersed in Class 1 water, DMEM and DMEM with 10% FBS, respectively. The 5th and 95th percentiles indicate nanoparticle suspensions that are mainly monodispersed. The size distribution curves are presented in Figure S1C.

The zeta potential values of the AuNPs-PAA and the AuNPs-PAA-Ctxb dispersed in Class 1 water were −30.53 mV and −29.27 mV, respectively. The zeta potential values shifted significantly towards less negative values when AuNPs-PAA and AuNPs-PAA-Ctxb were dispersed in DMEM (−8.03 mV and −7.59 mV, respectively) or in DMEM with 10% FBS (−8.37 mV and −7.04 mV, respectively).

The AuNPs-PAA(±Ctxb) used in the following experiments involving cell culture were dispersed in full medium containing 10% FBS. Table 2 presents a summary of the experiments, the exposure conditions and a short description of the results.

Cellular internalization of AuNPs-PAA-Ctxb

Cetuximab targets EGFR and thus can influence the interaction of AuNPs-PAA-Ctxb with the cells depending on their EGFR expression. Therefore, we verified the overexpression of EGFR in A431 cells by means of Western blot. Compared to A431 cells, HK-2 cells, THLE-2 cells and TIME cells displayed an EGFR expression of 26%, 3% and 2%, respectively. MDA-MB-453 cells had the lowest EGFR expression (0.14%) of all (Figure 1). TEM demonstrated the internalization of AuNPs-PAA-Ctxb in all cell types when exposed to 5.0 μg Au/mL of AuNPs-PAA-Ctxb for 3 h or 24 h (Figure 2). After an exposure period of 3 h, the nanoparticles were present in small intracellular membrane-bound vesicles, which were localized mostly in the peri-nuclear region of A431 cells (Figure 2A), HK-2 cells (Figure 2E) and THLE-2 cells (Figure 2G). In the EGFR-negative MDA-MB-453 cells, only a minimal uptake of nanoparticles was observed (Figure 2C). When the exposure period was increased to 24 h, the number of nanoparticle-containing vesicles and the amount of AuNPs-PAA-Ctxb in the vesicles appeared to increase in all cell types. The nanoparticle uptake by the TIME cells was characterized mainly by large clusters of AuNPs-PAA-Ctxb, which could be observed at both 3 h (Figure 2I) and 24 h of exposure (Figure 2J). EDS analysis on representative cells confirmed the presence of intracellular gold (Figure S2).

We also quantified the gold content of the cells by means of ICP-MS after incubation with 5.0 μg Au/mL of AuNPs-PAA(±Ctxb) for 3 h, 6 h, 12 h and 24 h (Figure 3). It is important to note that the ICP-MS data represents the interaction of AuNPs with the cell surface as well as the uptake of AuNPs by the cells. The results demonstrated maximum interaction of AuNPs-PAA-Ctxb with A431 cells after 3 h

Table 1 Characterization of the AuNPs-PAA and AuNPs-PAA-Ctxb dispersed in different media.

Suspension medium	Nanoparticle type	
	AuNPs-PAA	AuNPs-PAA-Ctxb
Modus size (nm) [5th and 95th percentile]		
Class 1 water	4 [4–14]	26 [13–53]
DMEM	5 [4–11]	25 [13–66]
DMEM +10% FBS	5 [4–11]	19 [12–62]
Zeta potential (mV) + SD		
Class 1 water	−30.53±0.25	−29.27±0.15
DMEM	−8.03±0.27	−7.59±0.45
DMEM +10% FBS	−8.37±0.25	−7.04±0.22

Notes: The size was measured with disc centrifugation. The values represent the modus particle size, the 5th and 95th percentile (nm). The zeta potential values were assessed with the Nanosizer Nano ZSP and are expressed as the mean nanoparticle surface charge ± standard deviation (n=3).
Abbreviations: AuNPs, gold nanoparticles; Ctxb, Cetuximab; DMEM, Dulbecco's modified Eagle's medium; FBS, fetal bovine serum; mV, millivolts; PAA, polyallylamine; SD, standard deviation.

(1.09±0.07 pg Au/cell). Then, the AuNPs-PAA-Ctxb content decreased to a plateau phase after 6 h, which continued until 24 h of exposure. During the plateau phase, there was no significant difference between AuNPs-PAA and AuNPs-PAA-Ctxb content (Figure 3A). The MDA-MB-453 cells showed a small, but significant increase in AuNPs-PAA content after 24 h (0.62±0.11 pg Au/cell) compared to 3 h of exposure (0.27±0.01 pg Au/cell) (Figure 3B). In HK-2 cells, the AuNPs-PAA(±Ctxb) content increased and peaked after 6 h of incubation (0.69±0.15 pg Au/cell for AuNPs-PAA and 0.98±0.07 pg Au/cell for AuNPs-PAA-Ctxb), after which it decreased gradually (Figure 3C). The THLE-2 cells demonstrated an increased AuNPs-PAA (±Ctxb) interaction after 24 h of exposure (0.51±0.02 pg Au/cell for AuNPs-PAA and 1.59±0.14 pg Au/cell for AuNPs-PAA-Ctxb) (Figure 3D). Finally, the TIME cells showed a trend of increasing AuNPs-PAA-Ctxb content after 12 h (0.38±0.07 pg Au/cell) (Figure 3E). Overall, the cellular AuNPs-PAA-Ctxb interaction was higher than the AuNPs-PAA interaction in TIME cells, in THLE-2 cells, in A431 cells after 3 h, in MDA-MB-453 cells after 3 h, and in HK-2 cells after 3 h and 6 h (exact p-values of 0.1).

AuNPs-PAA(±Ctxb) reduced the cell viability

TEM and ICP-MS results clearly showed interactions and uptake of AuNPs by the cells. Therefore, we assessed the cell viability after exposure to increasing concentrations of AuNPs-PAA(±Ctxb) for 3 h and 24 h. MTS assays revealed that AuNPs-PAA(±Ctxb) reduced cell viability in a concentration- and time-dependent manner (Figure 4). The lowest observed effect concentration (LOEC) presents the lowest tested concentration causing a significantly reduced cell viability. The LOEC of AuNPs-PAA after 3 h of exposure is 25.0 μg Au/mL for the A431 cells and 12.5 μg Au/mL for the MDA-MB-453 cells (Figure 4C), the THLE-2 cells (Figure 4G) and the TIME cells (Figure 4I). The HK-2 cells showed no significant reduction in cell viability (Figure 4E) at the maximum exposure concentration of 50.0 μg/mL. However, when the exposure period was increased to 24 h, the LOEC values decreased for all cell types (Table 3). Although exposure to AuNPs-PAA-Ctxb demonstrated a concentration- and time-dependent cytotoxicity profile comparable to that described for unconjugated AuNPs, they were significantly less cytotoxic. This difference in cytotoxic effect was generally observable from exposure to a nanoparticle concentration of 6.25 μg Au/mL for 24 h for A431 cells (Figure 4B), MDA-MB-453 cells (Figure 4D), HK-2 cells (Figure 4F) and THLE-2 cells (Figure 4H). Indeed, the calculated half maximal effect concentrations (EC_{50}) of AuNPs-PAA-Ctxb were significantly higher than the EC_{50} concentrations of AuNPs-PAA in all cell types, except for the TIME cells (Table 3). In addition, these EC_{50} values demonstrated that the cytotoxic effects of the nanoparticles were also cell type-dependent. Interestingly, the EGFR-overexpressing A431 cancer cells were the least sensitive cells. Amongst the healthy cells, the TIME cells were the most vulnerable for the cytotoxic effects of the AuNPs-PAA(±Ctxb), whereas the HK-2 cells were the most resistant.

AuNPs-PAA(±Ctxb) induced apoptosis

The MTS viability assays demonstrated reduced cell viability after exposure to AuNPs-PAA(±Ctxb). However, the assay is based on the metabolic activity of the cells and gives no further information about the process of cell death. Therefore, we performed live cell imaging measuring the caspase 3/7 activity and annexin V labeling, two markers of apoptosis. The results demonstrated that exposure to AuNPs-PAA(±Ctxb) caused apoptotic cell death in a concentration- and time-dependent manner (Figure 5). In the first 24 h, 50.0 μg Au/mL (red line) and 25.0 μg Au/mL (purple line) of AuNPs-PAA(±Ctxb) resulted in a significant increase in caspase 3/7 activity and annexin V labeling in all cell types. TIME cells, in addition, showed a significant increase in the apoptotic parameters after exposure to 12.5 μg Au/mL of nanoparticles (Figure 5I–T, yellow line).

Table 2 Overview of the performed cell assays, exposure conditions and results

Cell type	Endpoint	Assay	Incubation time	Concentration	Results
A431, MDA-MB-453, HK-2, THLE-2, TIME	EGFR expression	Western blot	N.A.	N.A.	Relative EGFR expression compared to A431: HK-2 ±26%; THLE-2 ±3%; TIME ±2%; MDA-MB-453 ±0.14%.
	AuNPs internalization	TEM	3 h, 24 h	5.0 µg Au/mL (Only AuNPs-PAA-Ctxb)	AuNPs-PAA-Ctxb in intracellular vesicles. AuNPs-PAA-Ctxb clusters in TIME cells.
		ICP-MS	3 h, 6 h, 12 h, 24 h	5.0 µg Au/mL	Fast AuNPs-PAA-Ctxb interaction in A431 and HK-2 cells followed by a decrease. AuNPs-PAA (±Ctxb) interaction progressively increased in TIME, THLE-2 and MDA-MB-453 cells. Overall, AuNPs-PAA-Ctxb interaction was higher than AuNPs-PAA interaction.
	Cell viability	MTS assay	3 h, 24 h	0–50.0 µg Au/mL	Conjugation of Ctxb to AuNPs-PAA reduced cytotoxicity. TIME cells were the most sensitive cells followed by THLE-2, MDA-MB-453, HK-2 and A431 cells.
	Apoptosis	Live cell imaging	0–72 h	0–50.0 µg Au/mL	AuNPs-PAA(±Ctxb) caused apoptosis, which increased with an increasing concentration and exposure period.
		+2 nM NAC	0–72 h	0–50.0 µg Au/mL	Annexin V and caspase 3/7 activity reduced when cells were co-exposed to NAC.
HK-2, THLE-2, TIME	Mitochondrial membrane depolarization	TMRM	3 h, 6 h, 12 h, 24 h	3.0–5.0 µg Au/mL	Mitochondrial membrane potential decreased most profoundly in TIME cells followed by THLE-2 cells and HK-2 cells after 12 h. Mitochondrial membrane potential recovers after 24 h.
		+2 nM NAC	12 h	3.0–5.0 µg Au/mL	NAC prevented mitochondrial membrane depolarization.
	Enzyme activity	Glutathione and thioredoxin reductase	12 h	3.0–5.0 µg Au/mL	GR and TrxR enzyme activity decreased most profoundly in TIME cells followed by THLE-2 cells and HK-2 cells.

Abbreviations: A431, human epidermoid cancer cells; AuNPs-PAA, polyallylamine-coated gold nanoparticles; Ctxb, Cetuximab; EGFR, epidermal growth factor receptor; HK-2, human kidney cells; ICP-MS, inductively coupled plasma mass spectrometry; MDA-MB-453, human breast cancer cells; MTS, 3-(4,5-dimethylthiazol-2-yl)-5-(3-carboxymethoxyphenyl)-2-(4-sulfophenyl)-2H-tetrazolium); N.A., not applicable; NAC, N-acetyl L-cysteine; THLE-2, human liver cells; TIME, human telomerase immortalized microvascular endothelial cells; TMRM, tetramethylrhodamine methyl ester; GR, glutathione reductase; TrxR, thioredoxin reductase; TEM, transmission electron microscopy.
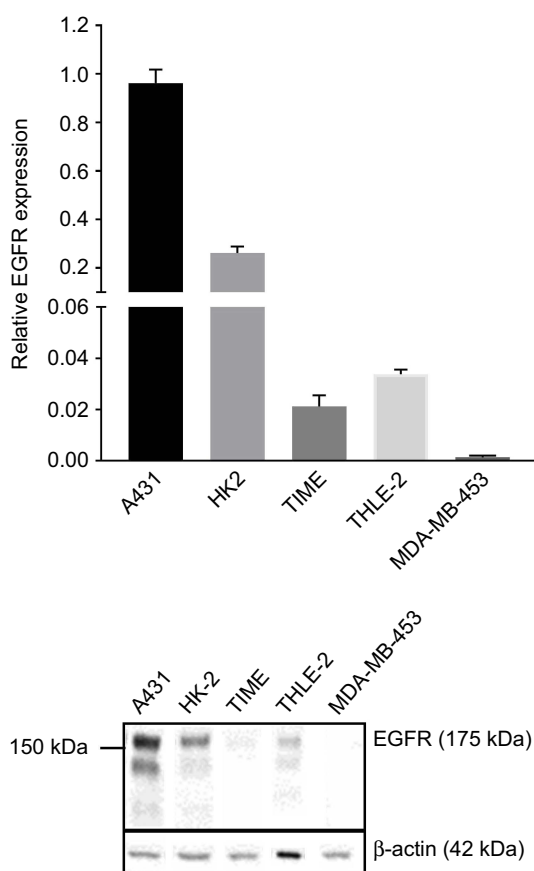
Figure I EGFR expression in HK-2 cells, THLE-2 cells, TIME cells and MDA-MB-453 cells relative to EGFR expression in A431 cells, determined by Western blot. Results are expressed as mean ± SE and are obtained from at least 4 independent replicates. Protein bands were normalized against β-actin.
Abbreviations: A431, human epidermoid cancer cells; EGFR, epidermal growth factor receptor; HK-2, human kidney cells; MDA-MB-453, human breast cancer cells; SE, standard error; THLE-2, human liver cells; TIME, human telomerase immortalized microvascular endothelial cells.

Extending the exposure period to 48 h, 12.5 µg Au/mL of AuNPs-PAA (yellow line) significantly increased apoptosis in MDA-MB-453 (Figure 5C–D) cells, HK-2 cells (Figure 5E–F) and THLE-2 cells (Figure 5G–H), whereas 6.25 µg Au/mL (brown line) also induced significant apoptosis in the TIME cells (Figure 5I–J) and HK-2 cells (Figure 5E–F). Finally, from 48 h to 72 h, 6.25 µg Au/mL of AuNPs-PAA (brown line) led to a significant number of apoptotic cells in MDA-MB-453 cells (Figure 5C–D), whereas 3.12 µg Au/mL of AuNPs-PAA (green line) increased apoptosis significantly in the TIME cells (Figure 5I–J). Similar to the MTS assay, the live cell imaging data demonstrated that AuNPs-PAA-Ctxb are less cytotoxic than the AuNPs-PAA. Exposure to AuNPs-PAA-Ctxb reduced or delayed the increase in caspase 3/7 activity and annexin V labeling compared to exposure to AuNPs-PAA.

AuNPs-PAA(±Ctxb) caused mitochondrial dysfunction

Live cell imaging identified apoptosis as the cell death mechanism after exposure to AuNPs-PAA(±Ctxb). Since mitochondria are key players in activating apoptosis, we assessed mitochondrial dysfunction by measuring the mitochondrial membrane potential after exposure of the cells to a sub-lethal concentration of AuNPs-PAA(±Ctxb) (Figure 6). A temporary hyperpolarization of the mitochondrial membrane potential was observed in HK-2 cells exposed to AuNPs-PAA-Ctxb (Figure 6A) and in TIME cells exposed to AuNPs-PAA(±Ctxb) (Figure 6C) for 3 h. Following 6 h of exposure to AuNPs-PAA(±Ctxb), the mitochondrial membrane potential of THLE-2 cells (Figure 6B) was reduced by approximately 11–14%, and of TIME cells (Figure 6C) by approximately 6–10%, compared to the unexposed controls. After extending the exposure period to 12 h, the mitochondrial membrane potentials of the THLE-2 cells and TIME cells were further depolarized to 80% and 60%, respectively. Only exposure to AuNPs-PAA could temporarily reduce the mitochondrial membrane potential of the HK-2 cells by 15% (Figure 6A). Finally, after 24 h of exposure, the mitochondrial membrane potential of the THLE-2 cells and the TIME cells was repolarized to more than 90% compared to the unexposed control cells. HK-2 cells exposed to AuNPs-PAA-Ctxb exhibited a significant hyperpolarization. Although AuNPs-PAA-Ctxb led to less cell death than AuNPs-PAA, no strong differences were observed in the mitochondrial membrane depolarization of cells exposed to AuNPs-PAA and those exposed to AuNPs-PAA-Ctxb.

AuNPs-PAA(±Ctxb) inhibited the activity of thioredoxin reductase and glutathione reductase

Thioredoxin reductase (TrxR) and glutathione reductase (GR) are enzymes involved in the antioxidant defense mechanism of the cell. TrxR and GR both use NADPH to reduce thioredoxin (Trx) and glutathione (GSH), respectively, which are in turn used by peroxidases to eliminate H_2O_2. Oxidative stress can have a negative effect on mitochondrial function. Since an exposure period of 12 h resulted in the most pronounced mitochondrial membrane depolarization (Figure 6), we measured the TrxR and GR activity in the cells after exposure to a non-lethal concentration of
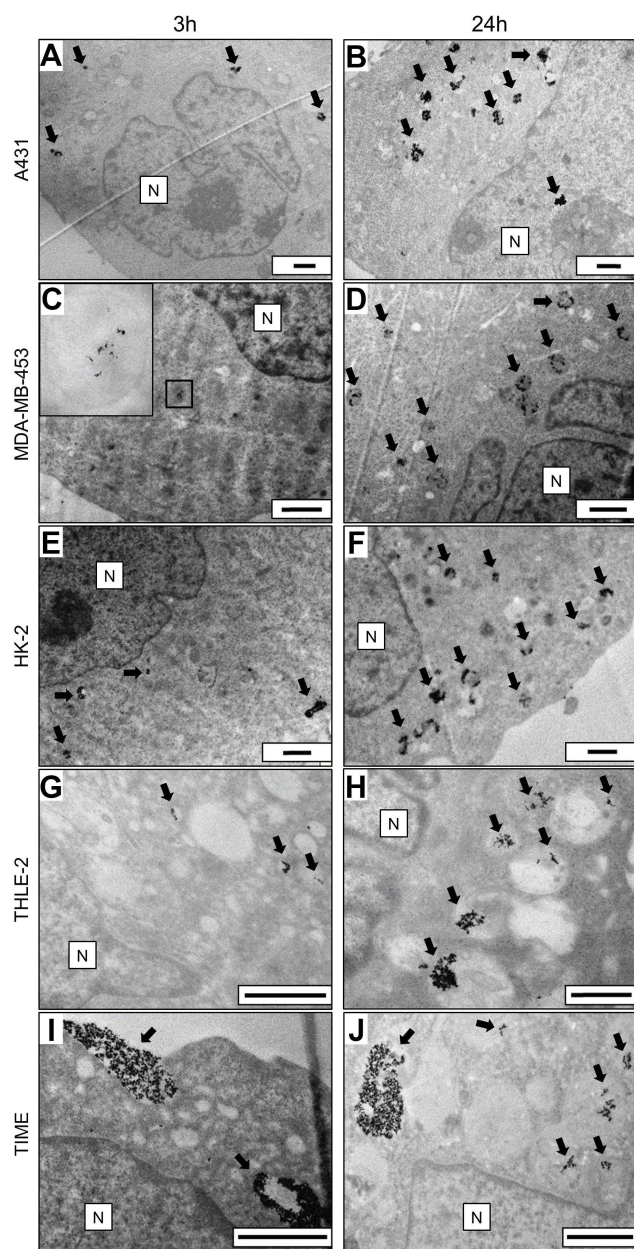
Figure 2 Transmission electron microscopy images demonstrating the internalization of AuNPs-PAA-Ctxb in A431 cells (**A** and **B**), MDA-MB-453 cells (**C** and **D**), HK-2 cells (**E** and **F**), THLE-2 cells (**G** and **H**) and TIME cells (**I** and **J**). The cells were exposed to 5.0 µg Au/mL of AuNPs-PAA-Ctxb for 3 h (left column) or 24 h (right column). Arrows indicate AuNPs-PAA-Ctxb. Images were acquired at different magnifications. Size bar =I µm, N = Nucleus.
Abbreviations: AuNPs-PAA-Ctxb, polyallylamine-coated gold nanoparticles conjugated to Cetuximab; A431, human epidermoid cancer cells; HK-2, human kidney cells; MDA-MB-453, human breast cancer cells, THLE-2, human liver cells; TIME, human telomerase immortalized microvascular endothelial cells.

AuNPs-PAA(±Ctxb) for 12 h (Figure 7). Incubation with AuNPs-PAA(±Ctxb) strongly inhibited the TrxR activity in HK-2 cells (Figure 7A), THLE-2 cells (Figure 7B) and TIME cells (Figure 7C) with residual activities of 22.8%, 15.3% and 6.3%, respectively. In addition, a decrease of the GR activity was observed, but to a lesser extent than was the case

for TrxR inhibition (with residual activities of 61.2%, 69.2% and 37.9% for HK-2 cells, THLE-2 cells and TIME cells, respectively). In general, the inhibitory effects on TrxR and GR were most profound in TIME cells, followed by THLE-2 cells and HK-2 cells.

The protective effect of N-acetyl L-cysteine (NAC)

Finally, we investigated the ability of NAC to counteract the cytotoxicity caused by AuNPs-PAA(±Ctxb). NAC is a potent thiol-containing anti-oxidant, which can interact with ROS such as OH^- and H_2O_2 through the reducing capacity of its thiol-disulfide exchange activity. Furthermore, NAC acts as a precursor of reduced glutathione.[45,46] Since an exposure period of 12 h resulted in the most pronounced mitochondrial membrane depolarization, the potential protective effect of NAC was assessed after exposure to a non-lethal concentration of AuNPs-PAA(±Ctxb) for 12 h. Co-incubation of the cells with AuNPs-PAA(±Ctxb) and NAC prevented mitochondrial membrane depolarization in all cell types after 12 h of exposure (Figure 6). Furthermore, the increases in caspase 3/7 activity and annexin V labeling were remarkably reduced (Figure 8) compared to AuNPs-PAA(±Ctxb) exposure without NAC (Figure 5). Indeed, during co-exposure with NAC, only exposure to the highest AuNPs-PAA(±Ctxb) concentrations of 50.0 µg Au/mL (red line) and 25.0 µg Au/mL (purple line) resulted in a significant increase in annexin V and caspase 3/7 labeling in most cell types. In addition, a concentration of 12.5 µg Au/mL (yellow line) of AuNPs-PAA resulted in a significant increase in annexin V and caspase 3/7 labeling in MDA-MB-453 cells (Figure 8C–D) and TIME cells (Figure 8I–J).

Correlation between cell viability, TrxR activity and mitochondrial membrane depolarization

The previous results demonstrated that the most sensitive TIME cells exhibited the strongest mitochondrial membrane depolarization, the highest basal TrxR activity and the strongest TrxR inhibition. Alternatively, the more resistant HK-2 cells showed a mild mitochondrial membrane depolarization, the lowest basal TrxR activity and the least TrxR inhibition. In order to interpret the relation between the cell viability, the TrxR activity and the mitochondrial membrane potential, correlation studies were performed. The results highlighted a clear correlation between: (1) the residual mitochondrial membrane potential and the cell viability (Figure 9A,
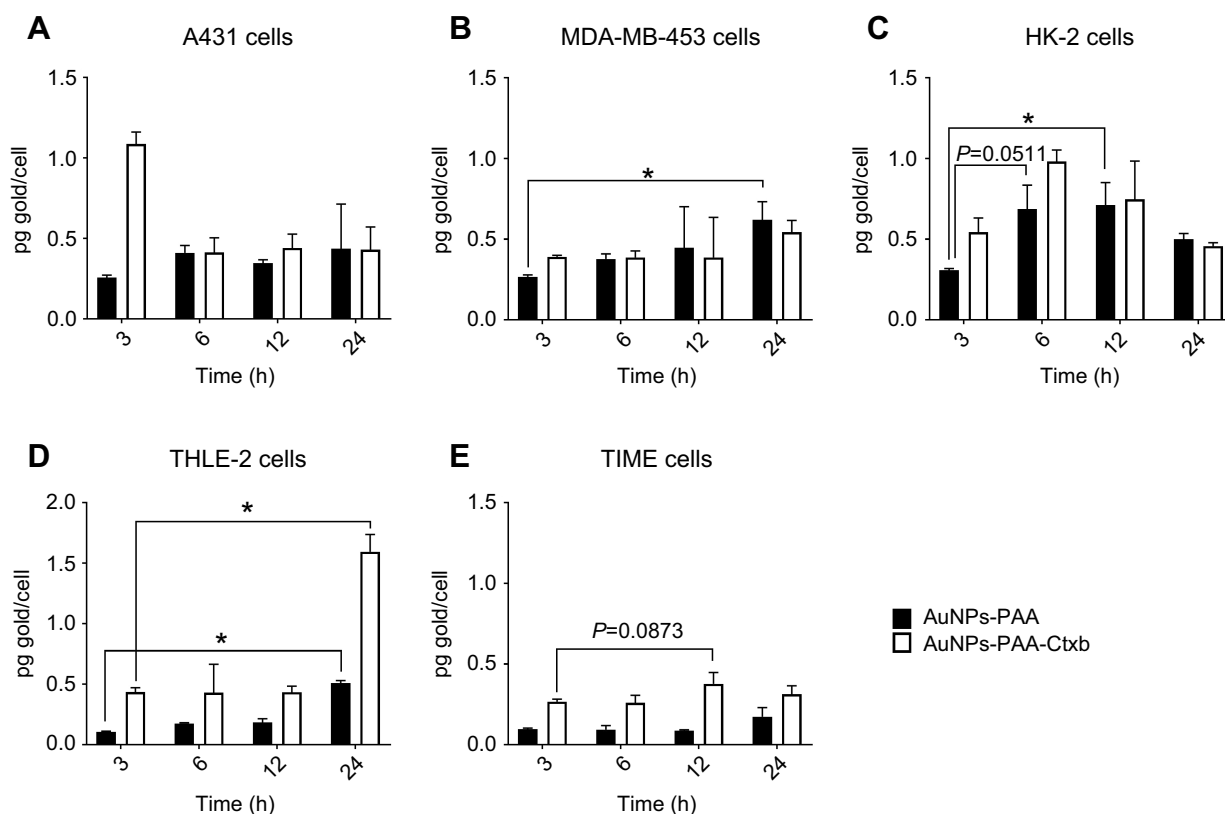
Figure 3 Interaction of AuNPs-PAA(±Ctxb) with A431 cells (**A**), MDA-MB-453 cells (**B**), HK-2 cells (**C**), THLE-2 cells (**D**) and TIME cells (**E**) quantified with ICP-MS. The cells were exposed to 5.0 µg Au/mL of AuNPs-PAA(±Ctxb) for 3 h, 6 h, 12 h or 24 h. Results are expressed as mean pg gold per cell ± SD calculated from 3 replicates per condition obtained from one experiment. A significant difference compared to 3 h of exposure was calculated by a Kruskal-Wallis test and a Dunn's post-hoc test (*$p<0.05$).
Abbreviations: A431, human epidermoid cancer cells; Ctxb, Cetuximab; Au, gold; AuNPs-PAA, polyallylamine-coated gold nanoparticles; HK-2, human kidney cells; ICP-MS, inductively coupled plasma mass spectrometry; MDA-MB-453, human breast cancer cells; SD, standard deviation; THLE-2, human liver cells; TIME, human telomerase immortalized microvascular endothelial cells.

Pearson's r =0.995), (2) basal TrxR activity and the cell viability (Figure 9B, Pearson's r =−0.929), (3) the extent of TrxR inhibition and the cell viability (Figure 9C, Pearson's r =−0.920), and (4) the extent of TrxR inhibition and the residual mitochondrial membrane potential (Figure 9D, Pearson's r =−0.997 for AuNPs-PAA and r =−0.969 for AuNPs-PAA-Ctxb).

Discussion

Only a limited number of reports have been published investigating the toxicity of AuNPs on non-cancerous human cells that were expected to be significantly exposed to AuNPs after in vivo administration. In this study, we presented a comprehensive evaluation of the cytotoxicity of polyallylamine-coated AuNPs conjugated to Cetuximab (AuNPs-PAA-Ctxb) in normal human kidney, liver and microvascular endothelial cells, and compared the toxicity profile with their unconjugated counterparts (AuNPs-PAA).

TEM images demonstrated that the AuNPs-PAA-Ctxb were present in intracellular vesicles and thus suggested that AuNPs-PAA-Ctxb uptake was mediated by endocytosis. The extent of nanoparticle internalization depends on the AuNPs surface modifications as well as on the cell type and the incubation time. Indeed, quantitative ICP-MS data showed that conjugation of the AuNPs-PAA with Cetuximab resulted in an overall increased cellular interaction. This was observed in the THLE-2 cells and TIME cells, but less so in the EGFR-negative MDA-MB-453 cells, which potentially use non-specific uptake routes. Furthermore, A431 cells and HK-2 cells, with high expression levels of EGFR, exhibited this higher AuNPs-PAA-Ctxb interaction, especially after short incubation times of 3 h and 6 h. This observation could be attributed to Cetuximab, since it promotes a fast receptor-mediated internalization of AuNPs in A431 cells and in pancreatic cancer cells after 30 min–2 h.[10,47] Furthermore, it has been demonstrated that intermediate-sized nanoparticles
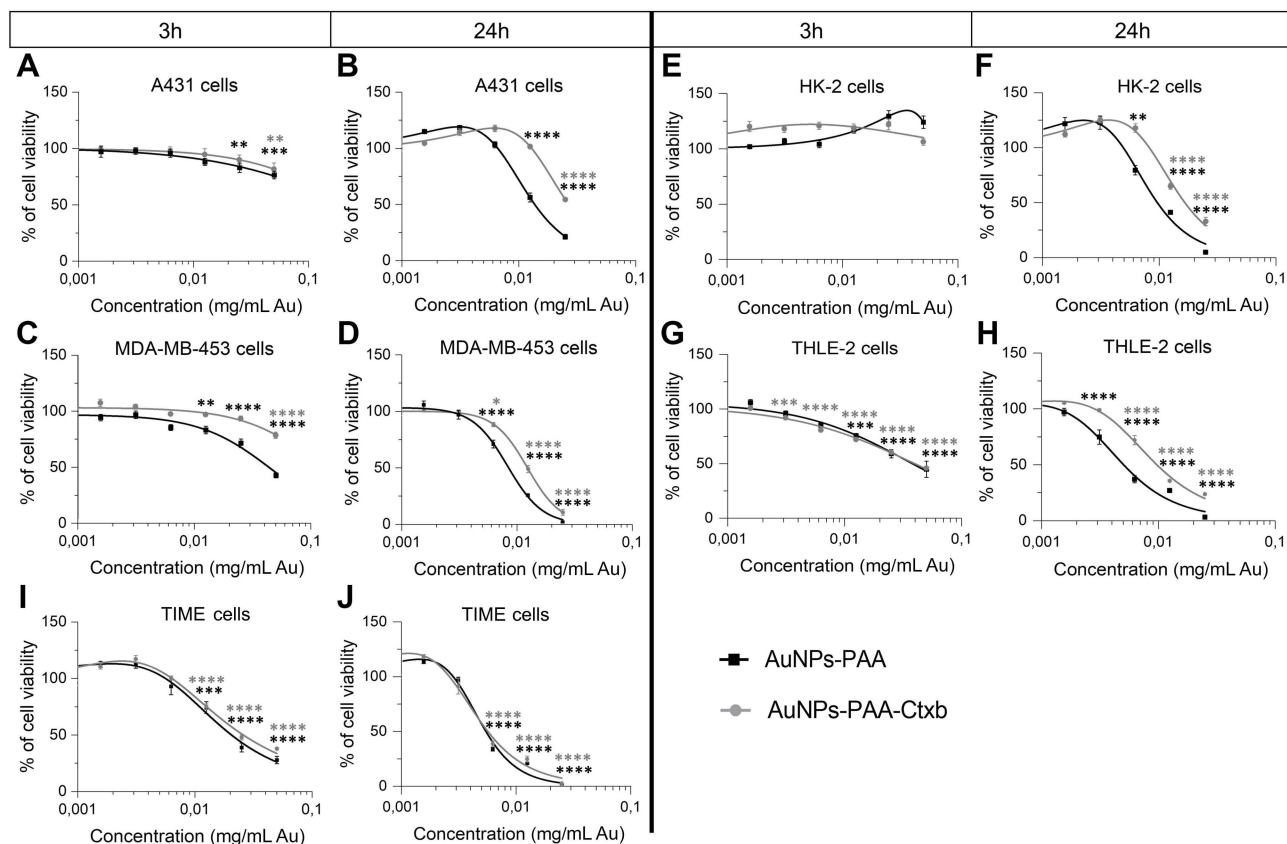
Figure 4 Cell viability after exposure to AuNPs-PAA (black curves) and AuNPs-PAA-Ctxb (gray curves) of A431 cells (**A** and **B**), MDA-MB-453 cells (**C** and **D**), HK-2 cells (**E** and **F**), THLE-2 cells (**G** and **H**) and TIME cells (**I** and **J**). Cells were exposed to increasing concentrations of AuNPs-PAA or AuNPs-PAA-Ctxb for 3 h or 24 h. The number of viable cells was assessed by MTS assay. The results are expressed as the mean percentage of viable cells relative to the unexposed cells ± SE and are obtained from at least three independent experiments with a minimum of three replicates per condition. A significantly reduced viability compared to the unexposed control was calculated by a one-way ANOVA and a Dunnett post-hoc test (*$p < 0.05$, **$p < 0.01$, ***$p < 0.001$ ****$p < 0.0001$).
Abbreviations: A431, human epidermoid cancer cells; ANOVA, analysis of variance; AuNPs-PAA, polyallylamine-coated gold nanoparticles; Ctxb, Cetuximab; HK-2, human kidney cells; MDA-MB-453, human breast cancer cells; MTS, 3-(4,5-dimethylthiazol-2-yl)-5-(3-carboxymethoxyphenyl)-2-(4-sulfophenyl)-2H-tetrazolium); SE, standard error; THLE-2, human liver cells; TIME, human telomerase immortalized microvascular endothelial cells.

Table 3 EC_{50} values after 24 h of cell exposure and LOEC after 3 h and 24 h of exposure to AuNPs-PAA and AuNPs-PAA-Ctxb.

| Cell type	AuNPs-PAA			AuNPs-PAA-Ctxb		
	LOEC (3 h)	LOEC (24 h)	EC_{50}+95% CI (24 h)	LOEC (3 h)	LOEC (24 h)	EC_{50}+95% CI (24 h)
A431	25.0	12.5	13.7 [12.8–14.6]	50.0	25.0	26.9 [24.8–29.1]
MDA-MB-453	12.5	6.25	8.31 [7.67–8.96]	50.0	6.25	12.3 [11.6–13.0]
HK-2	>50	6.25	9.65 [8.60–10.7]	>50	12.5	16.7 [15.3–18.2]
THLE-2	12.5	3.12	5.08 [4.36–5.79]	3.12	6.25	9.75 [9.04–10.5]
TIME	12.5	6.25	5.47 [5.18–5.75]	12.5	6.25	5.67 [5.08–6.26]

Note: Values were calculated from the MTS viability assays and expressed as μg Au/mL (Figure 4).
Abbreviations: A431, human epidermoid cancer cells; AuNPs, gold nanoparticles; CI, confidence interval; EC_{50}, Half maximal effect concentration; HK-2, human kidney cells; LOEC, Lowest observed effect concentration; MDA-MB-453, human breast cancer cells, THLE-2, human liver cells; TIME, human telomerase immortalized microvascular endothelial cells; Ctxb, cetuximab.

(20–60 nm) are endocytosed more efficiently than smaller nanoparticles.[48,49] Thus, in addition to receptor targeting, the overall increased size of the AuNPs-PAA-Ctxb com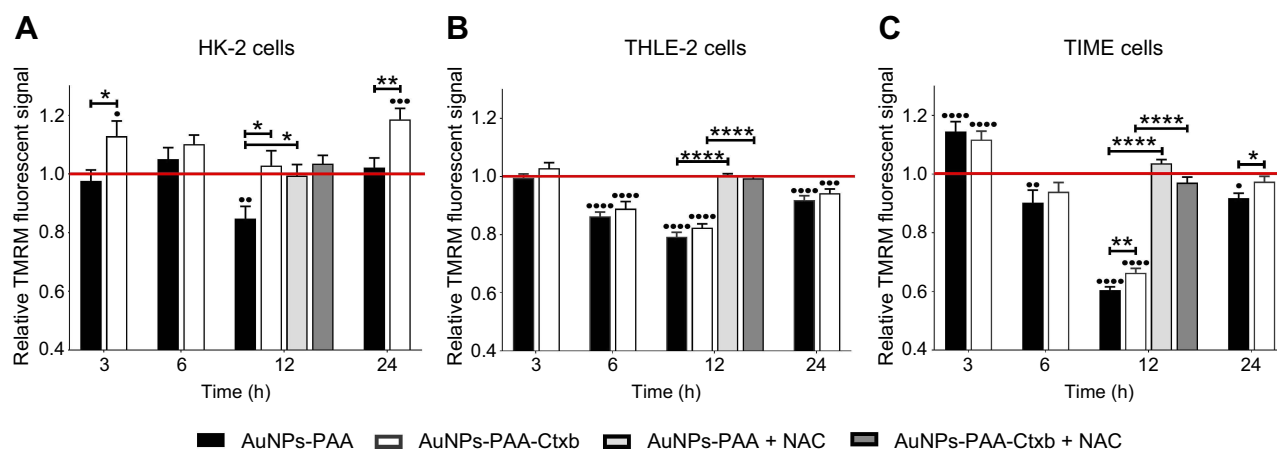pared to AuNPs-PAA could have facilitated their cellular uptake. However, we noticed a subsequent decrease in the gold content in the A431 and HK-2 cells. This could potentially be related to a reduced cell surface number of EGFR and/or exocytosis of the AuNPs. In fact,
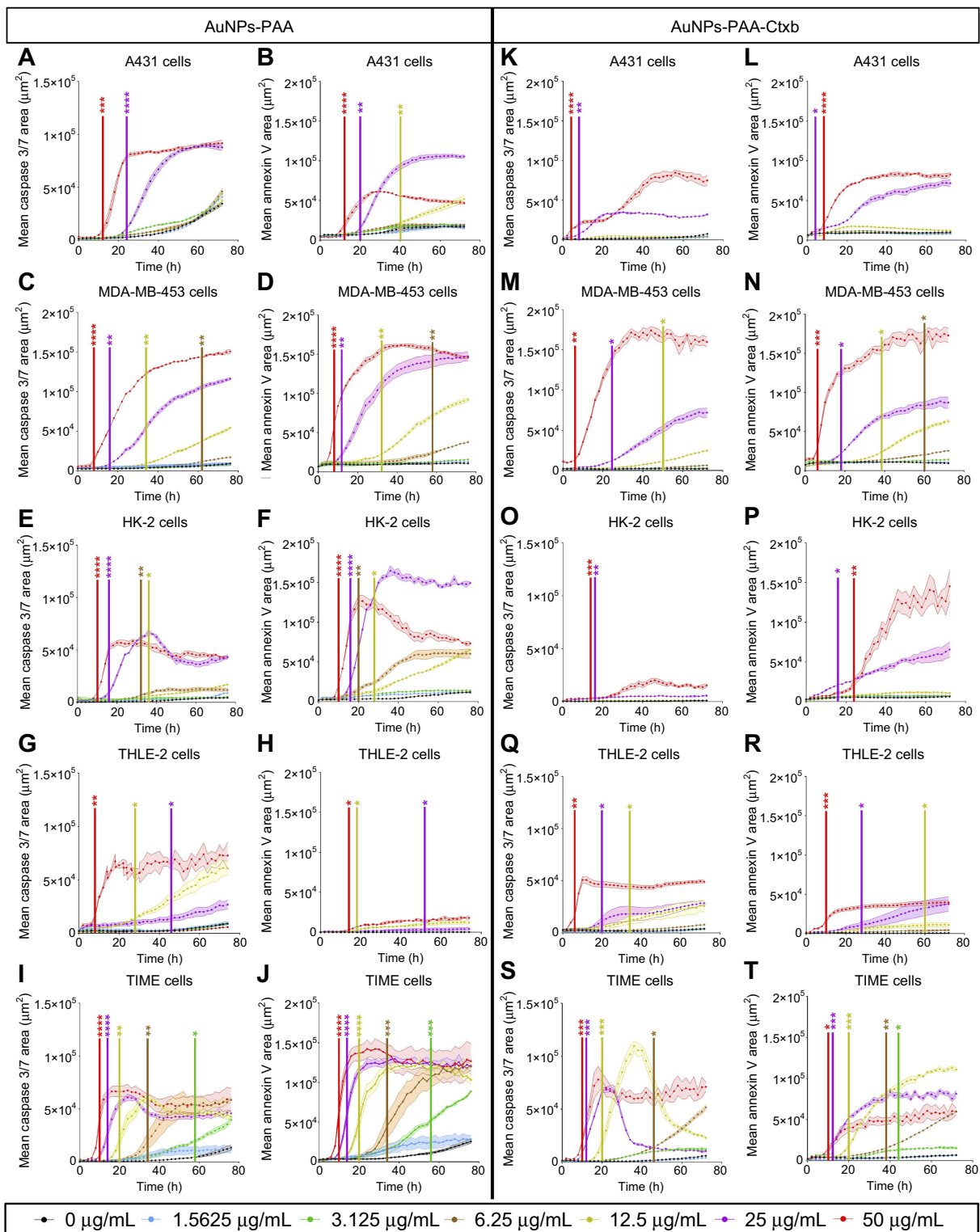
Figure 5 Live cell imaging for caspase 3/7 activation (left lanes) and annexin V labeling (right lanes) in A431 cells (**A** and **B, K** and **L**), MDA-MB-453 cells (**C** and **D, M** and **N**), HK-2 cells (**E** and **F, O** and **P**), THLE-2 cells (**G** and **H, Q** and **R**) and TIME cells (**I** and **J, S** and **T**). The cell lines were exposed to increasing concentrations of AuNPs-PAA or AuNPs-PAA-Ctxb. Time-lapse pictures were taken every 2 h for 72 h. The results are expressed as the mean area of caspase 3/7 or annexin V per well ± SE and are obtained from at least three replicates. A significant increase in caspase 3/7 activity and annexin V labeling compared to unexposed control cells was calculated by a two-way ANOVA and a Dunnett post-hoc test. The start of significance is visualized by vertical bars (*$p<0.05$, **$p<0.01$, ***$p<0.001$ ****$p<0.0001$).
Abbreviations: A431, human epidermoid cancer cells; ANOVA, analysis of variance; AuNPs-PAA, polyallylamine-coated gold nanoparticles; Ctxb, Cetuximab; HK-2, human kidney cells; MDA-MB-453, human breast cancer cells; SE, standard error; THLE-2, human liver cells; TIME, human telomerase immortalized microvascular endothelial cells.

Figure 6 Mitochondrial membrane potential measurements of the HK-2 cells (**A**), THLE-2 cells (**B**) and TIME cells (**C**) after exposure to AuNPs-PAA or AuNPs-PAA-Ctxb. TIME cells were exposed to 3.0 μg Au/mL, THLE-2 and HK-2 cells were exposed to 5.0 μg Au/mL of AuNPs-PAA or AuNPs-PAA-Ctxb. During the 12 h exposure, 2 nM NAC was added to assess oxidative stress. The mitochondrial membrane potential was measured with TMRM fluorescence, detected by flow cytometry. The results are expressed as mean TMRM fluorescent signal relative to the unexposed control cells (red line) ± SE and are obtained from at least three independent experiments with a minimum of three replicates per condition. Significant difference in TMRM signal compared to the unexposed control was calculated by a one-way ANOVA and a Dunnett post-hoc test (bullets). Significant difference in TMRM fluorescent signal between AuNPs-PAA and AuNPs-PAA-Ctxb exposed cells, or between nanoparticle-exposed cells and NAC co-exposed cells, was calculated by a Student's t-test (asterisks) (*$p<0.05$, **$p<0.01$, ***$p<0.001$ ****$p<0.0001$).
Abbreviations: ANOVA, analysis of variance; AuNPs-PAA, polyallylamine-coated gold nanoparticles; Ctxb, Cetuximab; HK-2, human kidney cells; NAC, N-acetyl L-cysteine; SE, standard error; THLE-2, human liver cells; TIME, human telomerase immortalized microvascular endothelial cells; TMRM, tetramethylrhodamine methyl ester.
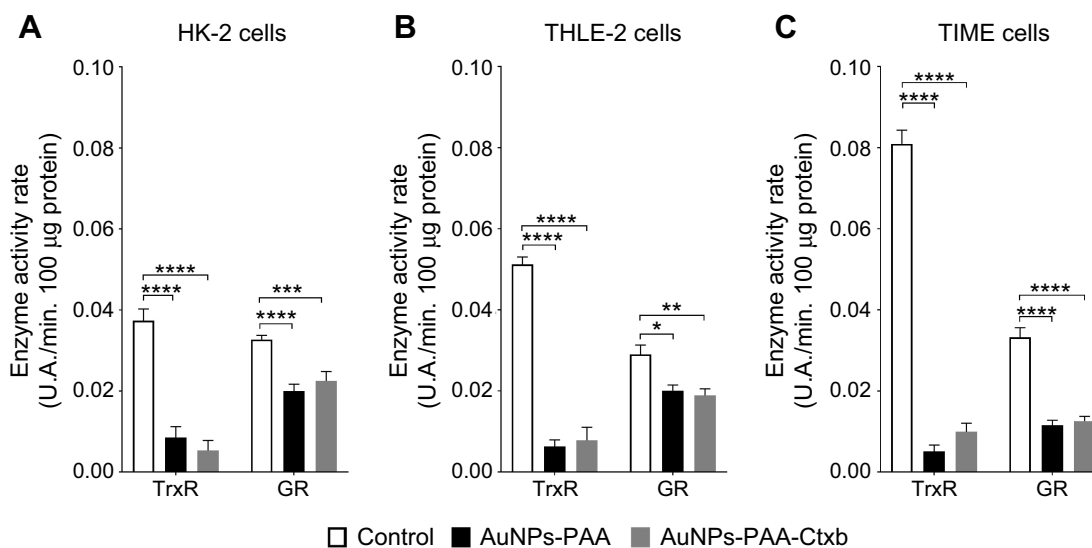

Figure 7 Thioredoxin reductase and glutathione reductase activity in the HK-2 cells (**A**), THLE-2 cells (**B**) and TIME cells (**C**) after exposure to AuNPs-PAA or AuNPs-PAA-Ctxb. TIME cells were exposed to 3.0 μg Au/mL, THLE-2 and HK-2 cells were exposed to 5.0 μg Au/mL of AuNPs-PAA or AuNPs-PAA-Ctxb for 12 h. The enzyme activity rate per minute was measured by the increase in absorbance at 405 nm for GR and at 412 nm for TrxR. The results are expressed as mean enzyme activity rate per minute per 100 μg of protein ± SE and are obtained from at least three independent experiments with a minimum of two replicates per condition. Significant difference in enzyme activity rate compared to the unexposed control was calculated by a Student's t-test (*$p<0.05$, **$p<0.01$, ***$p<0.001$ ****$p<0.0001$).
**Abbreviations:** AuNPs-PAA, polyallylamine-coated gold nanoparticles; Ctxb, Cetuximab; GR, Glutathione reductase; HK-2, human kidney cells; SE, standard error; THLE-2, human liver cells; TIME, human telomerase immortalized microvascular endothelial cells; TrxR, Thioredoxin reductase.

Cetuximab-conjugated AuNPs inhibit the recycling of EGFR from endosomes to the cell surface more efficiently than free Cetuximab.[10,47] This would lead to a prolonged reduction in the number of docking sites for Cetuximab and therefore less uptake of the AuNPs-PAA-Ctxb over time. Furthermore, it has been reported that macropinosomes in A431 cells diffuse with difficulty to lysosomes and travel back to the extracellular fluid.[50,51] No exocytosis processes were reported yet for HK-2 cells. In contrast to the aforementioned interaction kinetics, the MDA-MB-
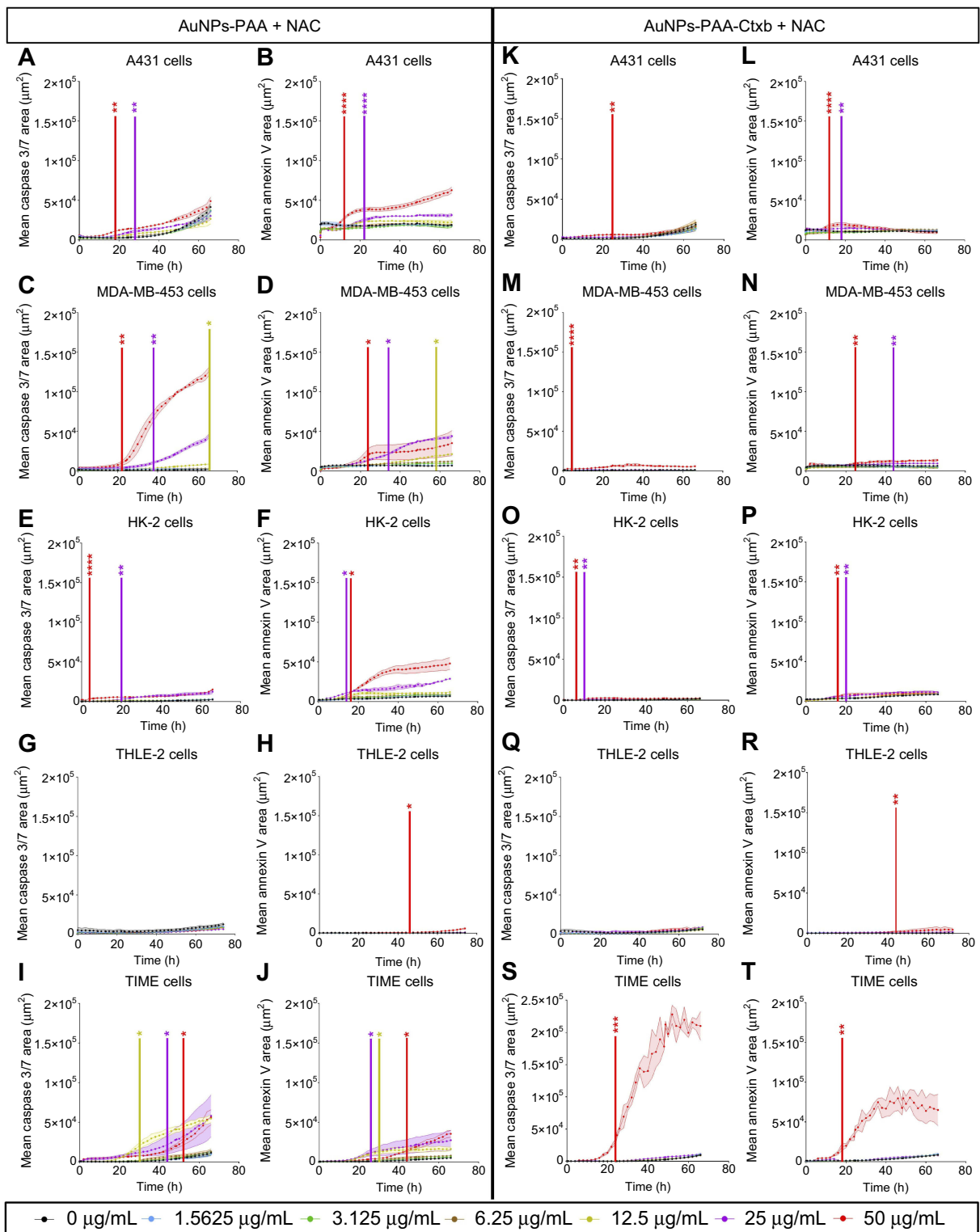
Figure 8 Live cell imaging for caspase 3/7 activation (left panels) and annexin V labeling (right panels) in A431 cells (**A** and **B**, **K** and **L**), MDA-MB-453 cells (**C** and **D**, **M** and **N**), HK-2 cells (**E** and **F**, **O** and **P**), THLE-2 cells (**G** and **H**, **Q** and **R**) and TIME cells (**I** and **J**, **S** and **T**). The cell lines were co-exposed to increasing concentrations of AuNPs-PAA or AuNPs-PAA-Ctxb and 2 nM of NAC. Time-lapse pictures were taken every 2 h for 72 h. The results are expressed as the mean area of caspase 3/7 or annexin V per well ± SE and are obtained from at least three replicates. A significant increase in caspase 3/7 activity and annexin V labeling compared to unexposed control cells was calculated by a two-way ANOVA and a Dunnett post-hoc test. The start of significance is visualized by vertical bars (*$p<0.05$, **$p<0.01$, ***$p<0.001$ ****$p<0.0001$).
Abbreviations: A431, human epidermoid cancer cells; ANOVA, analysis of variance; AuNPs-PAA, polyallylamine-coated gold nanoparticles; Ctxb, Cetuximab; HK-2, human kidney cells; MDA-MB-453, human breast cancer cells; SE, standard error; NAC, N-acetyl L-cysteine; THLE-2, human liver cells; TIME, human telomerase immortalized microvascular endothelial cells.
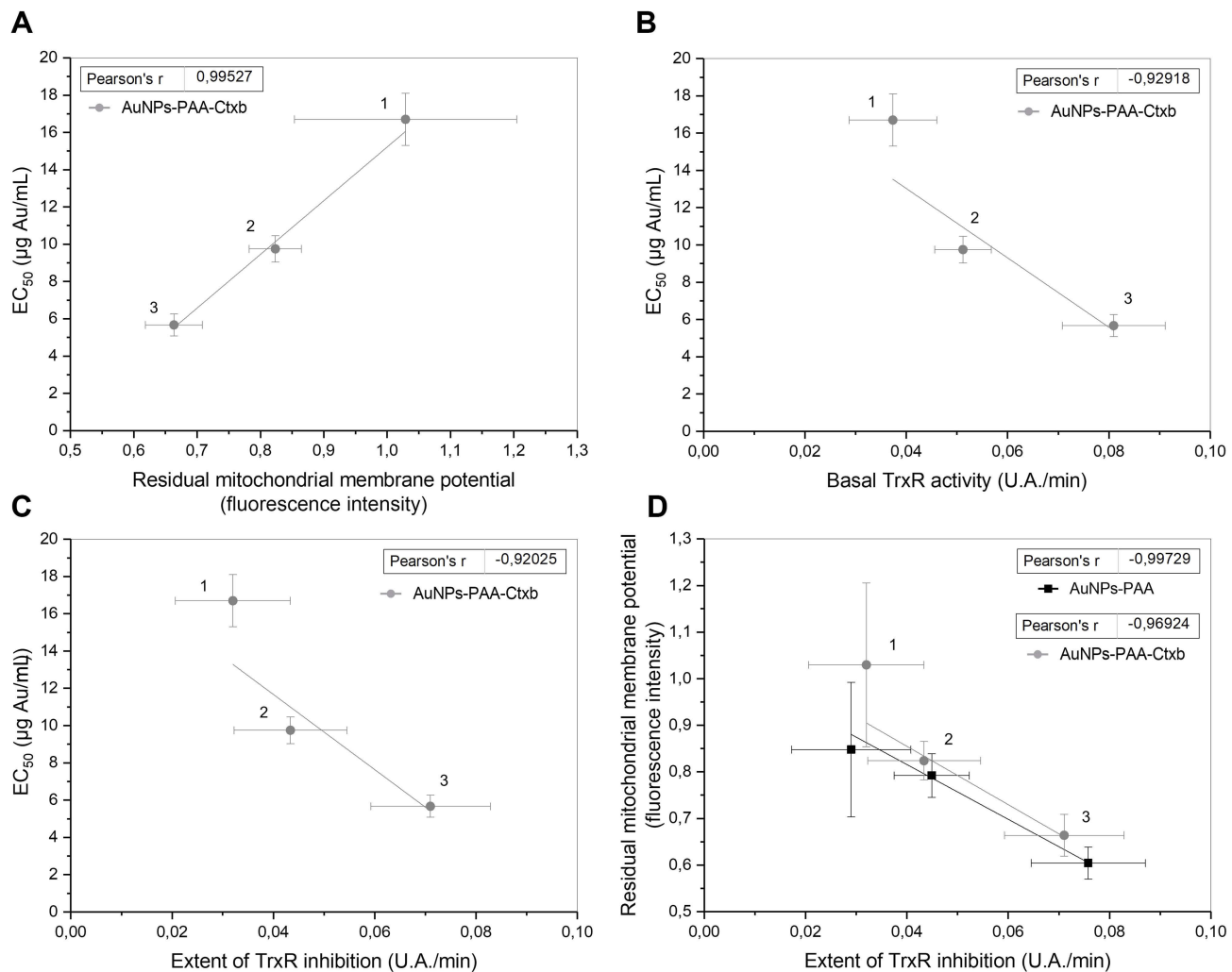
Figure 9 Correlation analyses showing the relation between the residual mitochondrial membrane potential and cell viability (**A**); the basal TrxR activity and cell viability (**B**); the extent of TrxR activity and cell viability (**C**); and the extent of TrxR inhibition and the residual mitochondrial potential (**D**). Data are presented as mean ± SD (for mitochondrial membrane potential and TrxR activity) or 95% CI (for EC_{50}). I= HK-2 cells, 2= THLE-2 cells and 3= TIME cells.
Abbreviations: CI, confidence interval; HK-2, human kidney cells; SD, standard deviation; THLE-2, human liver cells; TIME, human telomerase immortalized microvascular endothelial cells; TrxR, thioredoxin reductase; AuNPs-PAA, polyallylamine-coated gold nanoparticles; Ctxb, cetuximab; EC_{50}, half maximal effect concentration.

453 cells, the TIME cells and the THLE-2 cells showed a more gradual and progressive increase in AuNPs-PAA (±Ctxb) content with increasing incubation periods, which could indicate a less efficient and specific AuNPs uptake. Interestingly, despite the relatively low interactions of AuNPs-PAA(±Ctxb) with the TIME cells, as shown by ICP-MS (maximum 0.38±0.07 pg Au/cell), the TEM images demonstrated large intracellular nanoparticle clustering. Nanoparticle clustering was also observed in human umbilical vein endothelial cells (HUVECs) incubated with 10^{12} citrate-capped AuNPs/mL for 24 h under static conditions.[52] A possible hypothesis for this observation is that nanoparticles can be trapped and clustered within the glycocalyx coating of the endothelial cells.[53] Furthermore, the microvascular endothelial cells control

the continuous passage of macromolecules and fluid from the blood to the extravascular tissue. Therefore, endothelial cells are rich in cell surface invaginations to engulf proteins, lipids and nanoparticles.[54]

Since we demonstrated clear, but different interactions of the AuNPs-PAA(±Ctxb) with the cells, we performed cell viability assays to investigate the effects of AuNPs-PAA(±Ctxb) on the different cell types. Our results showed that the AuNPs-PAA(±Ctxb) toxicity was increased in a concentration- and time-dependent manner. In addition, the EC_{50} values, based on the MTS assays after 24 h of exposure, demonstrated that various cell types are differentially sensitive to the effects of the AuNPs. Interestingly, EGFR-overexpressing A431 cells exhibited the highest resistance to AuNPs-PAA-Ctxb-induced

toxicity (EC$_{50}$=26.9 µg Au/mL), followed by HK-2 cells (EC$_{50}$=16.7 µg Au/mL), MDA-MB-453 cells (EC$_{50}$=12.3 µg Au/mL), THLE-2 cells (EC$_{50}$=9.75 µg Au/mL) and TIME cells (EC$_{50}$=5.67 µg Au/mL). These findings are not consistent with several other toxicity studies demonstrating that cancer cells are more sensitive to nanoparticle-induced toxicity than normal cells and that antibody-conjugated AuNPs enhance cell death in antigen-overexpressing cancer cells.[13,55–59] In fact, we showed that conjugation of AuNPs-PAA to Cetuximab even reduced nanoparticle-induced cytotoxicity, leading to EC$_{50}$ values that are 1.5–2 times higher than the EC$_{50}$ values of the cells incubated with AuNPs-PAA. This observation could be attributed to the change in surface coating of AuNPs-PAA after antibody conjugation, which could reduce the interaction of gold with biological components.[36,60]

The calculated EC$_{50}$ values allow comparison of the sensitivity of the (normal) cells and the toxicity of our unique AuNPs-PAA(±Ctxb) with other reports in literature. As such, the EC$_{50}$ value of A431 cells after 24 h of exposure to AuNPs-PAA-Ctxb is 2.5 times lower than the EC$_{50}$ value calculated for 30 nm citrate-reduced AuNPs on A431 cells.[61] As a result, our AuNPs-PAA-Ctxb have a much higher capacity to induce cell death in the tumor cells, whereas the reduced cytotoxicity of the AuNPs-PAA-Ctxb compared to AuNPs-PAA is advantageous for the normal healthy cells. Focusing on the kidney cells, incubation of normal human proximal tubular cells (HPTCs) with 40 nm polyethylenimine-coated AuNPs has shown to activate pathways involved in apoptosis and DNA damage repair. An EC$_{50}$ value of 72.18 µg/mL was calculated after 24 h of exposure, which is approximately 4–7 times higher than the EC$_{50}$ value of the HK-2 cells in this study.[38] In the liver tissue, the RES is the main cause of rapid sequestration of AuNPs. Uptake of 5 nm polyvinylpyrrolidone-coated AuNPs (98 µg/mL) in endocytic vesicles was observed in hepatocytes of rat liver precision-cut slices.[62] This uptake did not translate into significant cytotoxicity after 24 h of exposure. The latter is consistent with 3.2 nm dihydrolipoic-coated gold nanoclusters (24.5 µg/mL) causing no toxicity in the normal human liver L02 cell line after 72 h of exposure.[62,63] In contrast, production of pro-inflammatory cytokines has been demonstrated in primary rat hepatocytes after 4 h of incubation with 20 nm AuNPs (211.2 µg/mL), showing a higher sensitivity than liver macrophages.[64] Furthermore, a time- and concentration-dependent uptake of 40 nm polyethylenimine-coated AuNPs in normal human hepatocytes resulted in oxidative stress. However, the calculated EC$_{50}$ value of 170 µg/mL

after 24 h of exposure is still 30 times higher than the EC$_{50}$ value for the THLE-2 cells in this study.[39] Finally, we showed that TIME cells exhibit the highest sensitivity to AuNPs-PAA(±Ctxb), which could be related to their clustered nanoparticle uptake observed by TEM imaging. It is noteworthy that the experiments were performed under static conditions, whereas the endothelial cell layer in particular is subjected to a continuous blood flow and shear stress in vivo. Fede et al (2015) revealed that the cytotoxicity of PEG-coated AuNPs in HUVECs was significantly lower under flow-conditions than under static conditions. However, the toxicity increased with increasing concentrations and incubation times, which is consistent with our data.[52] Altogether, our results regarding cell viability and the above-mentioned reports demonstrate that AuNPs-induced cytotoxicity depends on the cell type as well as on the nanoparticle size, coating, concentration and incubation time.

Multiple hypotheses have been proposed regarding how AuNPs interact with cellular components after endocytosis. For example, endosomal escape could lead to physical interaction between the AuNPs and biological components.[65,66] Others have reported on gold ion release due to particle degradation caused by the acidic lysosomal environment.[67–69] In order to gain knowledge regarding the underlying mechanisms of our AuNPs-PAA(±Ctxb) cytotoxicity, we assessed apoptosis, mitochondrial dysfunction and measured antioxidant enzyme activities. Our results demonstrated that AuNPs-PAA(±Ctxb) were able to decrease the TrxR and GR activity in normal cell types. Generally, the AuNPs-PAA(±Ctxb) inhibited TrxR more effectively than GR, which may be ascribed to the high affinity of gold for the selenocysteine residue present in the active site of TrxR, but lacking in GR.[70] TIME cells showed the highest basal TrxR and GR activity, followed by THLE-2 cells and HK-2 cells. The abundance of TrxR in TIME cells could be related to the Trx system modulating angiogenic activities, such as endothelial migration, proliferation and vascular network formation.[71,72] Consequently, AuNPs-PAA(±Ctxb) were able to exert a considerable stronger inhibitory effect on the TrxR (and GR) of TIME cells than on THLE-2 and HK-2 cells (6.3% of residual TrxR activity in TIME cells versus in 15.3% in THLE-2 cells and 22.8% in HK-2 cells). Similar cell type-dependent differences in TrxR inhibition were reported in 5 cancer cell lines with A431 cells, the most resistant cell type in our experiments, having the lowest basal TrxR activity.[67,68] Inhibition of TrxR and GR creates a lack of reduced Trx and GSH, which are needed as substrates for

peroxidases to eliminate H_2O_2. The disturbance in the thiol redox balance can lead to oxidative stress causing mitochondrial dysfunction.[73] Indeed, our results demonstrated a substantial depolarization of the mitochondrial membrane potential after 12 h of AuNPs incubation, especially in TIME cells (60.4% of control fluorescence), in THLE-2 cells (79.2% of control fluorescence) and to a lesser extent in HK-2 cells (84.8% of control fluorescence). Furthermore, a strong correlation was observed between the extent of TrxR inhibition and the mitochondrial membrane depolarization (Figure 9D). The correlation analyses including EC_{50} values (Figure 9A–C) indicate that the sensitivity of the cells to AuNPs-PAA(±Ctxb) was strongly associated with the basal TrxR activity, the extent of TrxR inhibition and the mitochondrial membrane depolarization. Alternatively, EGFR expression and cellular AuNPs-PAA (±Ctxb) interaction were less decisive, as shown by ICP-MS (maximum gold content of 0.98 pg/cell in HK-2 cells compared to 0.38 pg/cell in TIME cells).

Notably, the mitochondrial membrane depolarization recovered almost completely after 24 h of exposure to a sub-lethal concentration of AuNPs-PAA(±Ctxb). A possible explanation is given by Penninckx et al, who demonstrated a substantial increase of autophagic activity in A549 after 12–18 h of AuNPs incubation, but no longer after 24 h.[67] In addition, exposure to 50 nm citrate-capped AuNPs caused autophagy in HK-2 cells, promoting their cell survival.[74] This suggests that autophagy could be responsible for the observed cell recovery by providing energy through the lysosomal degradation of cytoplasmic constituents. However, next to serving as a cell survival mechanism, autophagy can also mediate the induction of apoptosis after exposure to AuNPs.[74] Furthermore, a link exists between apoptosis and the Trx system. More specifically, reduced Trx interacts with the apoptosis signaling kinase-1 (ASK-1) and prevents its homodimerization and activation. As Trx becomes oxidized, it dissociates from the complex and ASK1 induces the mitochondrial-dependent apoptotic pathway.[71,72] Since AuNPs-PAA(±Ctxb) caused a strong TrxR inhibition, it can lead to a lack of reduced Trx and a pro-apoptotic status. The live cell imaging results showed that exposure to AuNPs-PAA(±Ctxb) provoked a concentration-and time-dependent activation of caspase 3/7 and annexin V labeling, identifying apoptosis as a major mechanism of cell death.

We further verified the central role of oxidative stress in AuNPs-induced cytotoxicity by co-incubation of the cells with AuNPs-PAA(±Ctxb) and NAC. In addition to its antioxidant function, NAC acts as a precursor for reduced glutathione and can replenish the depleted intracellular glutathione content. The latter has been observed in human leukemia cells, human hepatoma cells and normal human fibroblasts following exposure to AuNPs.[75,76] The results showed that co-incubation of the cells with NAC avoided the mitochondrial membrane depolarization and significantly reduced apoptotic cell death. This is consistent with results demonstrating that pre-exposure of HeLa cells and MCF-7 cells with NAC, glutathione, and triphenylphosphine monosulfonate (TPPMS) increased cell survival during exposure to 1.4 nm TPPMS-coated AuNPs and 3–10 nm chitosan-coated AuNPs.[29,55] However, pre-exposure with ascorbic acid, a non-thiol containing antioxidant, did not significantly reduce the toxicity of the AuNPs. Therefore, Pan et al (2009) suggested that thiol-containing antioxidants not only reduced the oxidative stress caused by the nanoparticles, but also could neutralize the AuNPs interactions with vital biological targets.[29]

Altogether, our findings in normal cells complement other studies demonstrating that AuNPs disturb the cellular redox balance, trigger mitochondrial dysfunction and could lead to apoptosis in various cancer cells.[29,56–58,67–69,77–80] In fact, the inhibition of TrxR and the mitochondrial dysfunction have been identified as important biological aspects of the AuNPs radiosensitization mechanism in therapeutic radiotherapy.[68,78] Consequently, basal TrxR activity could possibly be used as a tool to estimate the sensitivity of normal cells to AuNPs when a significant accumulated dose of AuNPs is expected after administration. It should be noted that the results of this study are based on one specific cell line originating from either the kidney, the liver or the microvasculature, and therefore warrants further in vivo testing. Furthermore, this study stimulates future research to investigate AuNPs toxicity in normal human cells and tissues that encounter a significant dose of AuNPs after in vivo administration.

Conclusion

Since only a limited number of reports have been published investigating the toxicity of AuNPs on normal human cells, the present study complements the literature on the inhibitory effects of AuNPs investigated in cancer cells. The results of this study point out a general mechanism of cytotoxicity induced by AuNPs-PAA(±Ctxb). However, the sensitivity to AuNPs-PAA(±Ctxb) is cell-type dependent according to the cell type characteristics. More specifically, basal TrxR activity, TrxR inhibition and mitochondrial membrane depolarization were clearly correlated with the sensitivity of the cells to AuNPs-PAA

(±Ctxb). In contrast, EGFR expression and the subsequent cellular interactions with AuNPs-PAA(±Ctxb) were less clear cut. Furthermore, we demonstrated that conjugation to Cetuximab reduced the cytotoxicity of the AuNPs-PAA, potentially due to the change in surface coating. This study paves the way to investigate basal TrxR activity as a potential tool to predict which healthy cells and tissues could exhibit a high sensitivity to AuNPs after administration. This supports the understanding of the risks associated with the use of AuNPs in vivo.

Acknowledgments

Disclosure

References

1. Zhang X. Gold nanoparticles: recent advances in the biomedical applications. *Cell Biochem Biophys*. 2015;72(3):771–775. doi:10.1007/s12013-015-0529-4

2. Hainfeld JF, Slatkin DN, Focella TM, Smilowitz HM. Gold nanoparticles: a new X-ray contrast agent. *Br J Radiol*. 2006;79(939):248–253. doi:10.1259/bjr/13169882

3. Chang MY, Shiau AL, Chen YH, Chang CJ, Chen HH, Wu CL. Increased apoptotic potential and dose-enhancing effect of gold nanoparticles in combination with single-dose clinical electron beams on tumor-bearing mice. *Cancer Sci*. 2008;99(7):1479–1484. doi:10.1111/j.1349-7006.2008.00827.x

4. de Barros AB, Tsourkas A, Saboury B, Cardoso VN, Alavi A. Emerging role of radiolabeled nanoparticles as an effective diagnostic technique. *EJNMMI Res*. 2012;2(1):39. doi:10.1186/2191-219X-2-39

5. Geng F, Song K, Xing JZ, et al. Thio-glucose bound gold nanoparticles enhance radio-cytotoxic targeting of ovarian cancer. *Nanotechnology*. 2011;22(28):285101. doi:10.1088/0957-4484/22/28/285101

6. Hainfeld JF, Dilmanian FA, Zhong Z, Slatkin DN, Kalef-Ezra JA, Smilowitz HM. Gold nanoparticles enhance the radiation therapy of a murine squamous cell carcinoma. *Phys Med Biol*. 2010;55(11):3045–3059. doi:10.1088/0031-9155/55/11/004

7. Popovtzer R, Agrawal A, Kotov NA, et al. Targeted gold nanoparticles enable molecular CT imaging of cancer. *Nano Lett*. 2008;8(12):4593–4596.

8. Reuveni T, Motiei M, Romman Z, Popovtzer A, Popovtzer R. Targeted gold nanoparticles enable molecular CT imaging of cancer: an in vivo study. *Int J Nanomedicine*. 2011;6:2859–2864. doi:10.2147/IJN.S25446

9. Li S, Penninckx S, Karmani L, et al. LET-dependent radiosensitization effects of gold nanoparticles for proton irradiation. *Nanotechnology*. 2016;27(45):455101. doi:10.1088/0957-4484/27/36/365202

10. Bhattacharyya S, Bhattacharya R, Curley S, McNiven MA, Mukherjee P. Nanoconjugation modulates the trafficking and mechanism of antibody induced receptor endocytosis. *Proc Natl Acad Sci U S A*. 2010;107(33):14541–14546. doi:10.1073/pnas.1006507107

11. Kudgus RA, Walden CA, McGovern RM, Reid JM, Robertson JD, Mukherjee P. Tuning pharmacokinetics and biodistribution of a targeted drug delivery system through incorporation of a passive targeting component. *Sci Rep*. 2014;4:5669. doi:10.1038/srep05669

12. Karmani L, Bouchat V, Bouzin C, et al. (89)Zr-labeled anti-endoglin antibody-targeted gold nanoparticles for imaging cancer: implications for future cancer therapy. *Nanomedicine (Lond)*. 2014;9(13):1923–1937. doi:10.2217/nnm.13.185

13. Qian Y, Qiu M, Wu Q, et al. Enhanced cytotoxic activity of cetuximab in EGFR-positive lung cancer by conjugating with gold nanoparticles. *Sci Rep*. 2014;4:7490. doi:10.1038/srep07490

14. Moreau N, Michiels C, Masereel B, et al. PVD synthesis and transfer into water-based solutions of functionalized gold nanoparticles. *Plasma Processes Polym*. 2009;6:S888–S892. doi:10.1002/ppap.200932210

15. Karmani L, Labar D, Valembois V, et al. Antibody-functionalized nanoparticles for imaging cancer: influence of conjugation to gold nanoparticles on the biodistribution of 89Zr-labeled cetuximab in mice. *Contrast Media Mol Imaging*. 2013;8(5):402–408. doi:10.1002/cmmi.1539

16. Marega R, Karmani L, Flamant L. Antibody-functionalized polymer-coated gold nanoparticles targeting cancer cells: an *in vitro* and *in vivo* study. *J Mater Chem*. 2012;22(21305):21305–21312. doi:10.1039/c2jm33482h

17. Sonavane G, Tomoda K, Makino K. Biodistribution of colloidal gold nanoparticles after intravenous administration: effect of particle size. *Colloids Surf B Biointerfaces*. 2008;66(2):274–280. doi:10.1016/j.colsurfb.2008.07.004

18. Hirn S, Semmler-Behnke M, Schleh C, et al. Particle size-dependent and surface charge-dependent biodistribution of gold nanoparticles after intravenous administration. *Eur J Pharm Biopharm*. 2011;77(3):407–416. doi:10.1016/j.ejpb.2010.12.029

19. De Jong WH, Hagens WI, Krystek P, Burger MC, Sips AJ, Geertsma RE. Particle size-dependent organ distribution of gold nanoparticles after intravenous administration. *Biomaterials*. 2008;29(12):1912–1919. doi:10.1016/j.biomaterials.2007.12.037

20. Huang K, Ma H, Liu J, et al. Size-dependent localization and penetration of ultrasmall gold nanoparticles in cancer cells, multicellular spheroids, and tumors in vivo. *ACS Nano*. 2012;6(5):4483–4493. doi:10.1021/nn301282m

21. Huo S, Ma H, Huang K, et al. Superior penetration and retention behavior of 50 nm gold nanoparticles in tumors. *Cancer Res*. 2013;73(1):319–330. doi:10.1158/0008-5472.CAN-12-2071

22. England CG, Huang JS, James KT, Zhang G, Gobin AM, Frieboes HB. Detection of phosphatidylcholine-coated gold nanoparticles in orthotopic pancreatic adenocarcinoma using hyperspectral imaging. *PLoS One*. 2015;10(6):e0129172. doi:10.1371/journal.pone.0129172

23. Abdelhalim MA, Jarrar BM. The appearance of renal cells cytoplasmic degeneration and nuclear destruction might be an indication of GNPs toxicity. *Lipids Health Dis*. 2011;10:147. doi:10.1186/1476-511X-10-232

24. Abdelhalim MA, Jarrar BM. Renal tissue alterations were size-dependent with smaller ones induced more effects and related with time exposure of gold nanoparticles. *Lipids Health Dis*. 2011;10:163. doi:10.1186/1476-511X-10-232

25. Lasagna-Reeves C, Gonzalez-Romero D, Barria MA, et al. Bioaccumulation and toxicity of gold nanoparticles after repeated administration in mice. *Biochem Biophys Res Commun*. 2010;393 (4):649–655. doi:10.1016/j.bbrc.2010.02.046

26. Naz F, Koul V, Srivastava A, Gupta YK, Dinda AK. Biokinetics of ultrafine gold nanoparticles (AuNPs) relating to redistribution and urinary excretion: a long-term in vivo study. *J Drug Target*. 2016;24 (8):720–729. doi:10.3109/1061186X.2016.1144758

27. Gharatape A, Salehi R. Recent progress in theranostic applications of hybrid gold nanoparticles. *Eur J Med Chem*. 2017;138:221–233. doi:10.1016/j.ejmech.2017.06.034

28. Ng CT, Li JJ, Gurung RL, et al. Toxicological profile of small airway epithelial cells exposed to gold nanoparticles. *Exp Biol Med (Maywood)*. 2013;238(12):1355–1361. doi:10.1177/1535370213505964

29. Pan Y, Leifert A, Ruau D, et al. Gold nanoparticles of diameter 1.4 nm trigger necrosis by oxidative stress and mitochondrial damage. *Small*. 2009;5(18):2067–2076. doi:10.1002/smll.200900466

30. Li JJ, Hartono D, Ong CN, Bay BH, Yung LY. Autophagy and oxidative stress associated with gold nanoparticles. *Biomaterials*. 2010;31(23):5996–6003. doi:10.1016/j.biomaterials.2010.04.014

31. Chen YS, Hung YC, Liau I, Huang GS. Assessment of the in vivo toxicity of gold nanoparticles. *Nanoscale Res Lett*. 2009;4(8):858–864. doi:10.1007/s11671-009-9334-6

32. Terentyuk GS, Maslyakova GN, Suleymanova LV, et al. Circulation and distribution of gold nanoparticles and induced alterations of tissue morphology at intravenous particle delivery. *J Biophotonics*. 2009;2(5):292–302. doi:10.1002/jbio.200910005

33. Gosens I, Post JA, de la Fonteyne LJ, et al. Impact of agglomeration state of nano- and submicron sized gold particles on pulmonary inflammation. *Part Fibre Toxicol*. 2010;7(1):37. doi:10.1186/1743-8977-7-37

34. Abdelhalim MA, Jarrar BM. Gold nanoparticles induced cloudy swelling to hydropic degeneration, cytoplasmic hyaline vacuolation, polymorphism, binucleation, karyopyknosis, karyolysis, karyorrhexis and necrosis in the liver. *Lipids Health Dis*. 2011;10:166. doi:10.1186/1476-511X-10-232

35. Shukla R, Bansal V, Chaudhary M, Basu A, Bhonde RR, Sastry M. Biocompatibility of gold nanoparticles and their endocytotic fate inside the cellular compartment: a microscopic overview. *Langmuir*. 2005;21(23):10644–10654. doi:10.1021/la0513712

36. Alkilany AM, Murphy CJ. Toxicity and cellular uptake of gold nanoparticles: what we have learned so far? *J Nanopart Res*. 2010;12(7):2313–2333. doi:10.1007/s11051-010-9911-8

37. Connor EE, Mwamuka J, Gole A, Murphy CJ, Wyatt MD. Gold nanoparticles are taken up by human cells but do not cause acute cytotoxicity. *Small*. 2005;1(3):325–327. doi:10.1002/smll.200400093

38. Ortega MT, Riviere JE, Choi K, Monteiro-Riviere NA. Biocorona formation on gold nanoparticles modulates human proximal tubule kidney cell uptake, cytotoxicity and gene expression. *Toxicol in Vitro*. 2017;42:150–160. doi:10.1016/j.tiv.2017.04.020

39. Choi K, Riviere JE, Monteiro-Riviere NA. Protein corona modulation of hepatocyte uptake and molecular mechanisms of gold nanoparticle toxicity. *Nanotoxicology*. 2017;11(1):64–75. doi:10.1080/17435390.2016.1264638

40. Freese C, Gibson MI, Klok HA, Unger RE, Kirkpatrick CJ. Size- and coating-dependent uptake of polymer-coated gold nanoparticles in primary human dermal microvascular endothelial cells. *Biomacromolecules*. 2012;13(5):1533–1543. doi:10.1021/bm300248u

41. Wang JY, Chen J, Yang J, et al. Effects of surface charges of gold nanoclusters on long-term in vivo biodistribution, toxicity, and cancer radiation therapy. *Int J Nanomedicine*. 2016;11:3475–3485. doi:10.2147/IJN.S106073

42. Gunduz N, Ceylan H, Guler MO, Tekinay AB. Intracellular accumulation of gold nanoparticles leads to inhibition of macropinocytosis to reduce the endoplasmic reticulum stress. *Sci Rep*. 2017;7:40493. doi:10.1038/srep40493

43. Longmire M, Choyke PL, Kobayashi H. Clearance properties of nano-sized particles and molecules as imaging agents: considerations and caveats. *Nanomedicine (Lond)*. 2008;3(5):703–717. doi:10.2217/17435889.3.5.703

44. Li S, Bouchy S, Penninckx S, et al. Antibody-functionalized gold nanoparticles as tumor-targeting radiosensitizers for proton therapy. *Nanomedicine (Lond)*. 2019;14(3):317–333. doi:10.2217/nnm-2018-0161

45. Zafarullah M, Li WQ, Sylvester J, Ahmad M. Molecular mechanisms of N-acetylcysteine actions. *Cell Mol Life Sci*. 2003;60(1):6–20.

46. Aruoma OI, Halliwell B, Hoey BM, Butler J. The antioxidant action of N-acetylcysteine: its reaction with hydrogen peroxide, hydroxyl radical, superoxide, and hypochlorous acid. *Free Radic Biol Med*. 1989;6(6):593–597. doi:10.1016/0891-5849(89)90066-X

47. Garcia-Fernandez L, Garcia-Pardo J, Tort O, et al. Conserved effects and altered trafficking of Cetuximab antibodies conjugated to gold nanoparticles with precise control of their number and orientation. *Nanoscale*. 2017;9(18):6111–6121. doi:10.1039/c7nr00947j

48. Chithrani BD, Ghazani AA, Chan WC. Determining the size and shape dependence of gold nanoparticle uptake into mammalian cells. *Nano Lett*. 2006;6(4):662–668. doi:10.1021/nl052396o

49. Chithrani BD, Chan WC. Elucidating the mechanism of cellular uptake and removal of protein-coated gold nanoparticles of different sizes and shapes. *Nano Lett*. 2007;7(6):1542–1550. doi:10.1021/nl070363y

50. Hewlett LJ, Prescott AR, Watts C. The coated pit and macropinocytic pathways serve distinct endosome populations. *J Cell Biol*. 1994;124 (5):689–703. doi:10.1083/jcb.124.5.689

51. Hamasaki M, Araki N, Hatae T. Association of early endosomal autoantigen 1 with macropinocytosis in EGF-stimulated A431 cells. *Anat Rec A Discov Mol Cell Evol Biol*. 2004;277(2):298–306. doi:10.1002/ar.a.20027

52. Fede C, Fortunati I, Weber V, et al. Evaluation of gold nanoparticles toxicity towards human endothelial cells under static and flow conditions. *Microvasc Res*. 2015;97:147–155. doi:10.1016/j.mvr.2014.10.010

53. Cheng MJ, Kumar R, Sridhar S, Webster TJ, Ebong EE. Endothelial glycocalyx conditions influence nanoparticle uptake for passive targeting. *Int J Nanomedicine*. 2016;11:3305–3315. doi:10.2147/IJN.S106299

54. Wang Z, Tiruppathi C, Cho J, Minshall RD, Malik AB. Delivery of nanoparticle: complexed drugs across the vascular endothelial barrier via caveolae. *IUBMB Life*. 2011;63(8):659–667. doi:10.1002/iub.485

55. Martinez-Torres AC, Zarate-Trivino DG, Lorenzo-Anota HY, Avila-Avila A, Rodriguez-Abrego C, Rodriguez-Padilla C. Chitosan gold nanoparticles induce cell death in HeLa and MCF-7 cells through reactive oxygen species production. *Int J Nanomedicine*. 2018;13:3235–3250. doi:10.2147/IJN.S165289

56. Ramalingam V, Revathidevi S, Shanmuganayagam TS, Muthulakshmi L, Rajaram R. Gold nanoparticle induces mitochondria-mediated apoptosis and cell cycle arrest in nonsmall cell lung cancer cells. *Gold Bull*. 2017;50 (2):177–189. doi:10.1007/s13404-017-0208-x

57. Zhang F, Zhu X, Gong J, et al. Lysosome-mitochondria-mediated apoptosis specifically evoked in cancer cells induced by gold nanorods. *Nanomedicine (Lond)*. 2016;11(15):1993–2006. doi:10.2217/nnm-2016-0139

58. Wang L, Liu Y, Li W, et al. Selective targeting of gold nanorods at the mitochondria of cancer cells: implications for cancer therapy. *Nano Lett*. 2011;11(2):772–780. doi:10.1021/nl103992v

59. Kondath S, Srinivas Raghavan B, Anantanarayanan R, Rajaram R. Synthesis and characterisation of morin reduced gold nanoparticles and its cytotoxicity in MCF-7 cells. *Chem Biol Interact*. 2014;224:78–88. doi:10.1016/j.cbi.2014.09.025

60. Alex SA, Rajiv S, Chakravarty S, Chandrasekaran N, Mukherjee A. Significance of surface functionalization of gold nanorods for reduced effect on IgG stability and minimization of cytotoxicity. *Mater Sci Eng C Mater Biol Appl*. 2017;71:744–754. doi:10.1016/j.msec.2016.10.061

61. Choi SY, Jeong S, Jang SH, et al. In vitro toxicity of serum protein-adsorbed citrate-reduced gold nanoparticles in human lung adenocarcinoma cells. *Toxicol in Vitro*. 2012;26(2):229–237. doi:10.1016/j.tiv.2011.11.016

62. Dragoni S, Franco G, Regoli M, et al. Gold nanoparticles uptake and cytotoxicity assessed on rat liver precision-cut slices. *Toxicol Sci*. 2012;128(1):186–197. doi:10.1093/toxsci/kfs150

63. Yang Y, Nan J, Hou J, et al. Cytotoxicity of gold nanoclusters in human liver cancer cells. *Int J Nanomedicine*. 2014;9:5441–5448. doi:10.2147/IJN.S69013

64. Brown DM, Johnston H, Gubbins E, Stone V. Cytotoxicity and cytokine release in rat hepatocytes, C3A cells and macrophages exposed to gold nanoparticles–effect of biological dispersion media or corona. *J Biomed Nanotechnol*. 2014;10(11):3416–3429.

65. Zhang XQ, Xu X, Bertrand N, Pridgen E, Swami A, Farokhzad OC. Interactions of nanomaterials and biological systems: implications to personalized nanomedicine. *Adv Drug Deliv Rev*. 2012;64(13):1363–1384. doi:10.1016/j.addr.2012.08.005

66. Yang Y, Ren L, Wang H. Strategies in the design of gold nanoparticles for intracellular targeting: opportunities and challenges. *Ther Deliv*. 2017;8(10):879–897. doi:10.4155/tde-2017-0049

67. Penninckx S, Heuskin AC, Michiels C, Lucas S. The role of thioredoxin reductase in gold nanoparticle radiosensitization effects. *Nanomedicine (Lond)*. 2018. doi:10.2217/nnm-2018-0171

68. Penninckx S, Heuskin AC, Michiels C, Lucas S. Thioredoxin reductase activity predicts gold nanoparticle radiosensitization effect. *Nanomaterials*. 2019;9:2. doi:10.3390/nano9020295

69. Sabella S, Carney RP, Brunetti V, et al. A general mechanism for intracellular toxicity of metal-containing nanoparticles. *Nanoscale*. 2014;6(12):7052–7061. doi:10.1039/c4nr01234h

70. Saccoccia F, Angelucci F, Boumis G, et al. On the mechanism and rate of gold incorporation into thiol-dependent flavoreductases. *J Inorg Biochem*. 2012;108:105–111. doi:10.1016/j.jinorgbio.2011.11.005

71. Dunn LL, Buckle AM, Cooke JP, Ng MK. The emerging role of the thioredoxin system in angiogenesis. *Arterioscler Thromb Vasc Biol*. 2010;30(11):2089–2098. doi:10.1161/ATVBAHA.110.209643

72. Huang Q, Zhou HJ, Zhang H, et al. Thioredoxin-2 inhibits mitochondrial reactive oxygen species generation and apoptosis stress kinase-1 activity to maintain cardiac function. *Circulation*. 2015;131 (12):1082–1097. doi:10.1161/CIRCULATIONAHA.114.012725

73. Zorov DB, Juhaszova M, Sollott SJ. Mitochondrial ROS-induced ROS release: an update and review. *Biochim Biophys Acta*. 2006;1757(5–6):509–517. doi:10.1016/j.bbabio.2006.04.029

74. Ding F, Li Y, Liu J, et al. Overendocytosis of gold nanoparticles increases autophagy and apoptosis in hypoxic human renal proximal tubular cells. *Int J Nanomedicine*. 2014;9:4317–4330. doi:10.2147/IJN.S68685

75. Mateo D, Morales P, Avalos A, Haza AI. Oxidative stress contributes to gold nanoparticle-induced cytotoxicity in human tumor cells. *Toxicol Mech Methods*. 2014;24(3):161–172. doi:10.3109/15376516.2013.869783

76. Mateo D, Morales P, Avalos A, Haza AI. Comparative cytotoxicity evaluation of different size gold nanoparticles in human dermal fibroblasts. *J Exp Nanosci*. 2015;10(18):1401–1417. doi:10.1080/17458080.2015.1014934

77. Liu R, Wang Y, Yuan Q, An D, Li J, Gao X. The Au clusters induce tumor cell apoptosis via specifically targeting thioredoxin reductase 1 (TrxR1) and suppressing its activity. *Chem Commun (Camb)*. 2014;50(73):10687–10690. doi:10.1039/c4cc03320e

78. Taggart LE, McMahon SJ, Currell FJ, Prise KM, Butterworth KT. The role of mitochondrial function in gold nanoparticle mediated radiosensitisation. *Cancer Nanotechnol*. 2014;5(1):5. doi:10.1186/s12645-014-0005-7

79. Ghita M, McMahon SJ, Taggart LE, Butterworth KT, Schettino G, Prise KM. A mechanistic study of gold nanoparticle radiosensitisation using targeted microbeam irradiation. *Sci Rep*. 2017;7:44752. doi:10.1038/srep44752

80. Hwang-Bo H, Jeong JW, Han MH, et al. Auranofin, an inhibitor of thioredoxin reductase, induces apoptosis in hepatocellular carcinoma Hep3B cells by generation of reactive oxygen species. *Gen Physiol Biophys*. 2017;36(2):117–128. doi:10.4149/gpb_2016043

Supplementary materials
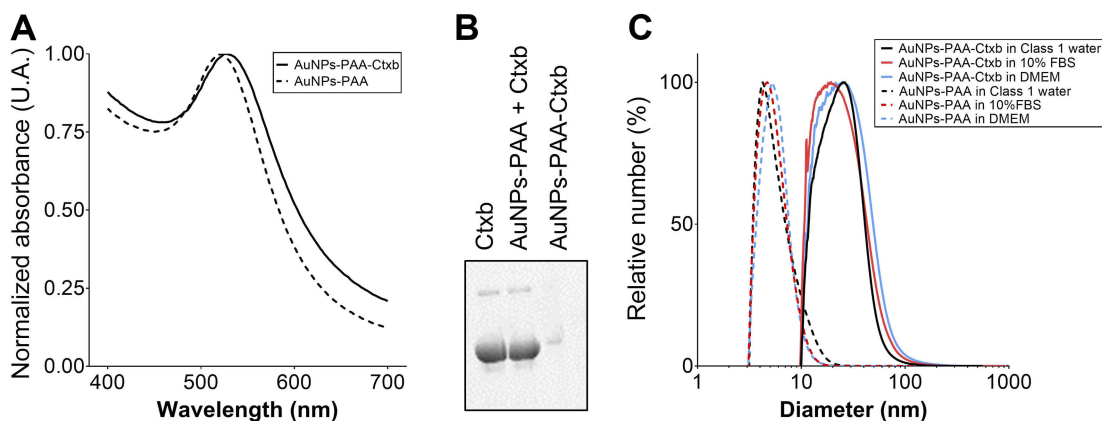
Figure S1 UV-Vis spectrum of AuNPs-PAA and AuNPs-PAA-Ctxb (**A**). Gel electrophoresis of Ctxb, AuNPs-PAA + Ctxb and AuNPs-PAA-Ctxb (**B**). Size distribution curves (relative number) of AuNPs-PAA and AuNPs-PAA-Ctxb in Class 1 water, DMEM and DMEM +10% FBS obtained from CPS Disk Centrifugation (Benelux Scientific, Eke, Belgium) (**C**).
Abbreviations: AuNPs-PAA, polyallylamine-coated gold nanoparticles; Ctxb, Cetuximab; FBS, Fetal bovine serum; DMEM, Dulbecco's Modified Eagle Medium.

$$y = \frac{k}{1 + \left(\frac{x}{x_{50}}\right)^s}$$

Equation S1 Log-logistic function for curve fitting of the MTS viability data.

$$y = \frac{k(1 + gx)}{1 + (1 + 2gx_{50})\left(\frac{x}{x_{50}}\right)^s}$$

Equation S2 Modified log-logistic function for curve fitting of the MTS viability data.

In both equations, y represents the experimental cell viability, x is the gold concentration and ^{s} defines the slope parameter. Moreover, k is the response at x=0 and x_{50} is the gold concentration at which the cell viability is reduced by 50% compared to control response. Finally, in the second equation, g represents the hormesis parameter, modelling a potential stimulatory effect of low gold concentrations.

A THLE-2 cells – 24h
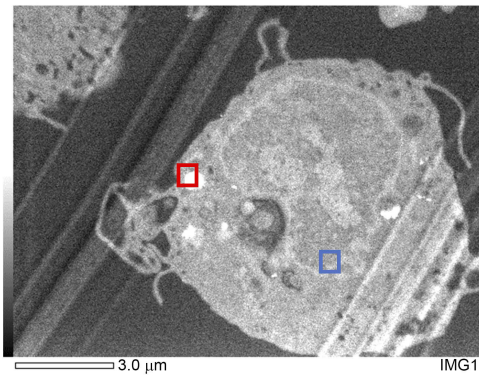
B
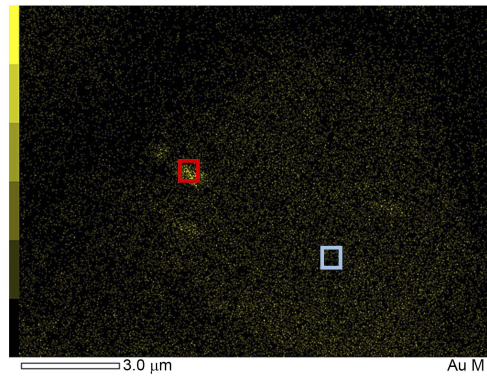
C

D

E ZAF method standardless quantitative analysis
Fitting coefficient: 0.6856

Element	(keV)	Mass%	Error%	Atom%	K
C K	0.277	71.65	0.24	83.91	73.34
O K	0.525	17.42	1.51	15.31	12.28
Au M	2.121	10.93	1.54	0.78	14.38
Total		100		100	

F ZAF method standardless quantitative analysis
Fitting coefficient: 0.7333

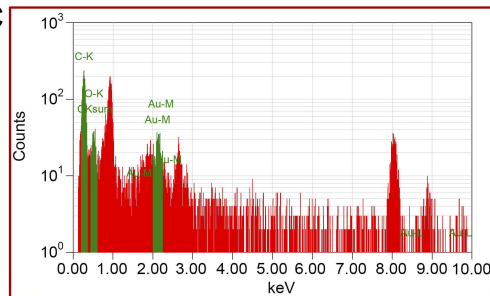| Element	(keV)	Mass%	Error%	Atom%	K
C K	0.277	76.05	0.32	80.88	85.38
O K	0.525	23.95	2.48	19.12	14.62
Au M					
Total		100		100	

TIME cells – 24h

G

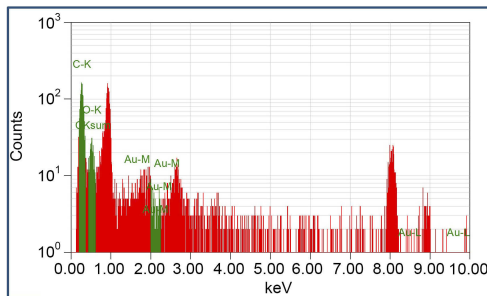

H

I

J

K ZAF method standardless quantitative analysis
Fitting coefficient: 0.4868

Element	(keV)	Mass%	Error%	Atom%	K
C K	0.277	73.77	0.12	86.31	75.00
O K	0.525	14.65	0.78	12.86	9.86
Au M	2.121	11.58	0.76	0.83	15.14
Total		100		100	

L ZAF method standardless quantitative analysis
Fitting coefficient: 0.4286

Element	(keV)	Mass%	Error%	Atom%	K
C K	0.277	79.47	0.09	83.75	88.56
O K	0.525	20.53	0.74	16.25	11.44
Au M					
Total		100		100	

M HK-2 cells – 3h

N

O

P

Q ZAF method standardless quantitative analysis
Fitting coefficient: 0.4868

Element	(keV)	Mass%	Error%	Atom%	K
C K	0.277	73.04	0.07	79.75	80.72
O K	0.525	24.51	0.50	20.09	16.40
Au M	2.121	2.45	0.54	0.16	2.88
Total		100		100	

R ZAF method standardless quantitative analysis
Fitting coefficient: 0.4286

Element	(keV)	Mass%	Error%	Atom%	K
C K	0.277	73.36	0.06	78.58	82.58
O K	0.525	26.64	0.47	21.42	17.42
Au M					
Total		100		100	

Figure S2 Energy dispersive X-ray spectroscopy analysis on a representative THLE-2 cell (**A**), a TIME cell (**G**) and a HK-2 cell (**M, N**), which were treated with 5 µg Au/mL of AuNPs-PAA-Ctxb for 3 h or 24 h. Gold mapping was performed on the THLE-2 cell (**B**) and the TIME cell (**H**). Bright signal zones (red squares) were analyzed resulting in specific X-ray spectra (**C**, **I**, **O**) and quantification of gold, carbon and oxygen (**E**, **K**, **Q**). No-signal zones (blue squares) were analyzed resulting in specific X-ray spectra (**D**, **J**, **P**) and the detection of only carbon and oxygen (**F**, **L**, **R**).

International Journal of Nanomedicine

Publish your work in this journal

The International Journal of Nanomedicine is an international, peer-reviewed journal focusing on the application of nanotechnology in diagnostics, therapeutics, and drug delivery systems throughout the biomedical field. This journal is indexed on PubMed Central, MedLine, CAS, SciSearch®, Current Contents®/Clinical Medicine, Journal Citation Reports/Science Edition, EMBase, Scopus and the Elsevier Bibliographic databases. The manuscript management system is completely online and includes a very quick and fair peer-review system, which is all easy to use. Visit http://www.dovepress.com/testimonials.php to read real quotes from published authors.

Submit your manuscript here: https://www.dovepress.com/international-journal-of-nanomedicine-journal